iLogDemons: A Demons-Based Registration Algorithm for Tracking Incompressible Elastic Biological Tissues

Tommaso Mansi · Xavier Pennec · Maxime Sermesant · Hervé Delingette · Nicholas Ayache

Abstract Tracking soft tissues in medical images using non-linear image registration algorithms requires methods that are fast and provide spatial transformations consistent with the biological characteristics of the tissues. LogDemons algorithm is a fast non-linear registration method that computes diffeomorphic transformations parameterised by stationary velocity fields. Although computationally efficient, its use for tissue tracking has been limited because of its *adhoc* Gaussian regularisation, which hampers the implementation of more biologically motivated regularisations. In this work, we improve the logDemons by integrating elasticity and incompressibility for soft-tissue tracking. To that end, a mathematical justification of demons Gaussian regularisation is proposed. Building on this result, we replace the Gaussian smoothing by an efficient elastic-like regulariser based on isotropic differential quadratic forms of vector fields. The registration energy functional is finally minimised under the divergence-free constraint to get incompressible deformations. As the elastic regulariser and the constraint are linear, the method remains computationally tractable and easy to implement. Tests on synthetic incompressible deformations showed that our approach outperforms the original logDemons in terms of elastic incompressible deformation recovery without reducing the image matching accuracy. As an application, we applied the proposed algorithm to estimate 3D myocardium strain on clinical cine MRI of two adult patients. Results showed that incompressibility constraint improves the cardiac motion recovery when compared to the ground truth provided by 3D tagged MRI.

T. Mansi, X. Pennec, M. Sermesant, H. Delingette and N. Ayache
INRIA Sophia Antipolis Méditerranée, Asclepios Research Project
2004 Route des Lucioles - BP 93, 06902 Sophia Antipolis, France
Tel.: +33.4.92.38.71.56
Fax: +33.4.92.38.76.69
E-mail: Tommaso.Mansi@inria.fr

1 Introduction

Tissue tracking in sequences of medical images is an important task in many clinical applications, either for disease diagnosis or therapy guidance. However there is no easy way to achieve this, even with user input. A standard approach is to use non-linear image registration to estimate dense spatial transformations between images. For instance, cardiac motion is estimated by non-linearly co-registering the frames of a cardiac sequence, yielding a dense displacement field that quantifies the myocardium motion (Bistoquet et al, 2008).

In practice, non-linear image registration is performed by minimising a dissimilarity criterion between the images to register up to a regularisation term that models prior knowledge about the spatial transformations. For clinical applications, the impenetrability of matter must be ensured, i.e. transformations must be smooth one-to-one mappings. In addition, the transformations must be consistent with the properties of the tissue to track, such as elasticity and incompressibility. This is all the more important if the estimated deformations are used to analyse anatomical changes between different time points (Ashburner et al, 1998). However, adding these constraints to image registration algorithms are often achieved at the price of computational complexity. In this paper, an efficient non-linear registration algorithm based on the fast demons approach is proposed for tracking elastic and incompressible soft tissues.

1.1 Diffeomorphic Non-Linear Image Registration

With the recent advances in computational anatomy, mathematical frameworks based on diffeomorphic deformations have been developed to estimate one-to-one differentiable mappings between the images to register. One of the most successful method is to encode deformations using B-splines. Diffeomorphic deformation is ensured by limiting the motion to 40% of the distance between knots (Rueckert et al, 2006) but this injectivity condition on spline transformations (Choi and Lee, 2000) prevents from accessing diffeomophisms with very large deformations.

Another approach is to parameterise the transformations by velocity fields according to the Lagrange transport equation (Arnold, 1989). When the velocity fields vary over time, large diffeomorphic deformations can be estimated using the Large Deformation Diffeomorphic Metric Mappings (LDDMM) (Miller et al, 2002; Beg et al, 2005). Nonetheless, complex partial differential equations must be solved to integrate the velocity field over time along a geodesic path, resulting in high computational cost.

This limitation can be tackled using *stationary* velocity fields, which are integrated very efficiently through exponential maps (Arsigny et al, 2006a; Bossa et al, 2007; Hernandez et al, 2009). Although such a parameterisation cannot capture all the diffeomorphisms, the stationarity of the velocity appears to be appropriate for biological deformations from an empirical point of view (see Ashburner (2007); Vercauteren et al (2008, 2009); Peyrat et al (2009); Yeo et al (2009); Hernandez et al (2009); Lorenzi et al (2010) for instance). In particular, Hernandez et al (2009) showed that there are no significant differences between time-varying and stationary velocity fields when registering brain MRI.

Among the methods based on stationary velocities, *logDemons* (Vercauteren et al, 2008) is an efficient non-linear registration algorithm based on the demons optimisation (Thirion, 1998). Two images are registered by alternating an optimisation step, which updates the stationary velocity field in a voxel-wise manner, and a Gaussian smoothing step, which models a diffusion motion. LogDemons algorithm is appealing as it ensures diffeomorphic mappings, it enables to work on velocities and transformations simultaneously and its complexity is linear in the number of voxels. However, the diffusion prior may not be appropriate for tracking biological tissues as it has no physical meaning. If mathematical justifications of demons optimisation step have been provided (Cachier et al, 2003; Vercauteren et al, 2009), theoretical foundations of the Gaussian regularisation still has to be consolidated (Pennec et al, 1999; Modersitzki, 2004; Cahill et al, 2009). This paper presents a mathematical justification of demons Gaussian regularisation which enables to estimate *elastic* and *incompressible* deformations.

1.2 Elastic Non-Linear Image Registration

First introduced by Broit (1981), elastic registration algorithms consist in regularising the transformations with the linear elasticity equation, also known as the Lamé equation. Although computationally efficient, these regularisers are suitable for small displacements only as they can yield deformation overlaps and discontinuities in their derivatives (Modersitzki, 2004). Techniques based on smooth elastic body splines have been developed (Rueckert et al, 1999; Sorzano et al, 2005). Yet, they are computationally demanding and diffeomorphic mappings are ensured through *ad-hoc* penalisation of the registration energy (Rueckert et al, 2006; DeCraene et al, 2009), which makes the computation of the inverse transformation critical. Cachier and Ayache (2004) demonstrated that the linear Lamé equation is actually a specific first order isotropic differential quadratic form (IDQF) of the transformation. High order IDQF can be designed, resulting in elastic-like regularisation of any order of smoothness. Cachier and Ayache (2004) also conjectured a separable elastic-like vector filter that behaves like an IDQF of infinite order. This filter has been used in demons algorithms in place of the Gaussian kernel (Cachier and Ayache, 2004; Mansi et al, 2009). However, its link with IDQF energies is not clear. In this paper we investigate how this filter relates to the IDQF to rigorously integrate it in the logDemons regularisation energy.

1.3 Incompressible Non-Linear Image Registration

Incompressible deformations cannot be recovered with elastic regularisers alone; explicit constraints must be added. A transformation is volume-preserving if its Jacobian determinant equals one. This constraint is non-linear and requires *ad-hoc* numerical schemes that are computationally demanding (Rohlfing et al, 2003; Haber and Modersitzki, 2004). Bistoquet et al (2008) proposed to use the linear approximation of that constraint, i.e. the divergence of the displacements is null. However, volume drifts appear when deformations become large, which the authors controlled by penalising the energy functional.

When estimating fluid motion, incompressibility is satisfied if the velocity is divergence-free. Building up on this observation, countless optical flow techniques (Horn and Schunck, 1981) based on the continuity equation and the divergence-free constraint have been developed to estimate incompressible fluid motion from 3D images (see (Heitz et al, 2009) and reference therein). Song and Leahy (1991) and Gorce et al (1997) applied this approach to estimate 3D cardiac velocity from 4D CT images. Cuzol et al (2007) combined the optical flow algorithm with the Helmholtz decomposition to estimate 2D fluid motion parameterised by divergence-free and curl-free parameter maps. Saddi et al (2007) constrained

a fluid registration algorithm to be incompressible by projecting the update velocities onto the space of divergence-free vector fields using Helmholtz decomposition. All these techniques showed satisfying results and demonstrated that incompressibility constraints can improve the estimation of incompressible fluid motion. However, the fluid model may not be suitable for tracking elastic biological tissues: the incompressibility condition on the transformation is usually preferred for biological applications.

Interestingly, one can demonstrate that diffeomorphisms parameterised by divergence-free velocity fields through the transport equation are incompressible (Evans, 1998). Hinkle et al (2009) for instance used this property to reconstruct images of incompressible organ with LDDMM and divergence-free time varying velocity fields. In this paper we rely on this property to integrate the incompressibility constraint in the logDemons algorithm.

1.4 Model-Based Non-Linear Image Registration

For tracking biological tissues, some authors have proposed to guide non-linear registration algorithms with biomechanical models that incorporate more details about the underlying tissues and improve the previously described linear elasticity regularisers. These approaches have been successfully applied in cardiac motion estimation (Papademetris et al, 2000; Sinusas et al, 2001; Veress et al, 2005; Phatak et al, 2009; Sundar et al, 2009a) and brain shift estimation (Ferrant et al, 2001; Clatz et al, 2005). However, the underlying models often rely on physical parameters that are difficult to determine for a given patient. Besides, such models may not apply anymore in pathological cases. Finally, they require meshing the space domain by unstructured grids in order to solve complex partial differential equations. For all these reasons we prefer here a purely image-driven algorithm.

1.5 Aim and Paper Organisation

This paper proposes a consistent and efficient framework for elastic incompressible non-linear registration based on the logDemons algorithm. Contrary to our previous work (Mansi et al, 2009), this approach operates entirely in the log-domain. The constraint is strong and is applied directly in the demons minimisation space. After a brief introduction to the logDemons algorithm (Sec. 2), we propose a mathematical justification of demons Gaussian regularisation that enables to adapt the algorithm to other transformation models (Sec. 3). We then replace that regulariser with multi-order IDQF whose minimiser is exactly computed with Cachier and Ayache (2004) elastic-like vector filter. Finally, strong incompressibility is ensured by constraining the stationary velocity fields that parameterise the transformations to be

divergence-free (Sec. 4). Our method, hereafter termed *iLogDemons*, is mathematically consistent as all its elements and parameters are controlled. The proposed demons framework results in the following advantages with respect to previous techniques: *i)* the elastic regulariser and the incompressibility constraint are linear, yielding low computational overhead, *ii)* they are rigorously integrated in the demons energy functional, yielding closed form minimisers that can be easily disabled by the user and applied to subdomains of the images, and *iii)* the incompressibility constraint is strongly enforced: no volume drifts appear. Sec. 5 reports results on synthetic datasets with known ground truth. As a clinical application, we employed the iLogDemons to estimate myocardium motion and strain on clinical cine MR images of the heart of two adult patients with heart failure. In both experiments, the iLogDemons improved the recovery of incompressible transformations compared with the original logDemons.

2 Background: Log-Domain Diffeomorphic Demons

Proposed by (Vercauteren et al, 2008), log-domain diffeomorphic demons algorithm, hereafter termed *logDemons*, is an efficient non-linear registration algorithm based on the demons approach (Thirion, 1998). Given a reference image R and a template image T defined over the domain $\Omega \subset \mathbb{R}^d$ (typically $d = 3$), logDemons estimates a dense spatial transformation $\phi : \Omega \to \mathbb{R}^d$ that best aligns T to R. This is achieved by alternating an *optimisation step*, which updates the transformation in a voxel-wise manner, and a *regularisation step*, which traditionally consists in Gaussian smoothing. Cachier et al (2003) justified the demons algorithm by the alternate minimisation of the energy functional:

$$\mathscr{E}(\phi, \phi_c) = \frac{\|R - T \circ \phi_c\|_{L_2}^2}{\lambda_i^2} + \frac{\text{dist}(\phi_c, \phi)}{\lambda_x^2} + \frac{\|\nabla\phi\|_{L_2}^2}{\lambda_d^2} \qquad (1)$$

ϕ is the dense spatial transformation to estimate. $\phi_c : \Omega \to \mathbb{R}^d$ is an intermediate transformation, called *correspondences*, that matches the two images under an uncertainty controlled by λ_x^2 without considering the regularity of the transformation. The first term of (1) is the similarity criterion or data-term. It measures how R and $T \circ \phi_c$ are similar. λ_i^2 relates to the noise in the images. The last term of (1) is the regulariser whose strength is controlled by λ_d^2. It ensures the spatial smoothness of the transformation ϕ, here by penalising large gradients, and models prior knowledge about the transformation to recover. The second term of (1) couples the correspondences ϕ_c with the smooth transformation ϕ. This term unifies in a common mathematical framework the optimisation step, which amounts to minimising $\mathscr{E}(\phi, \phi_c)$ with respect to ϕ_c, and the regularisation step, which consists in minimising $\mathscr{E}(\phi, \phi_c)$ with respect to ϕ.

In logDemons, the registration energy (1) is adapted to estimate spatial transformations that are parameterised by *stationary* velocity fields $\mathbf{v} : \Omega \to \mathbb{R}^d$ through the exponential map $\phi = \exp(\mathbf{v})$. Such transformations belong to the subspace of diffeomorphisms $\mathbb{G}$ generated by the one-parameter subgroups of diffeomorphisms. The space of velocities V is the *log-domain*. As $\mathbf{v}$ is stationary, $\exp(\mathbf{v})$ is efficiently computed using the "scaling-and-squaring" algorithm proposed by Arsigny et al (2006a) (Appendix A). Alternatively, ϕ can be defined as the solution of the Lagrange transport equation: $\partial\phi(\mathbf{x},t)/\partial t = \mathbf{v}(\phi(\mathbf{x},t))$, $\phi(\mathbf{x},0) = \mathbf{x}$. With $\phi = \exp(\mathbf{v})$ and $\phi_c = \exp(\mathbf{v}_c)$, the logDemons energy writes in the log-domain:

$$\mathscr{E}(\mathbf{v},\mathbf{v}_c) = \frac{1}{\lambda_i^2} \|R - T \circ \exp(\mathbf{v}_c)\|_{L_2}^2 +$$
$$\frac{1}{\lambda_x^2} \|\log(\exp(-\mathbf{v}) \circ \exp(\mathbf{v}_c))\|_{L_2}^2 + \frac{1}{\lambda_d^2} \|\nabla\mathbf{v}\|_{L_2}^2 \quad (2)$$

The optimisation step minimises $\mathscr{E}(\mathbf{v},\mathbf{v}_c)$ with respect to $\mathbf{v}_c$. The correspondence field ϕ_c is modelled with the diffeomorphic update rule $\phi_c = \exp(\mathbf{v}_c) = \phi \circ \exp(\delta\mathbf{v})$, where ϕ is the current estimate of the transformation to recover and $\delta\mathbf{v}$ is an unknown small update velocity field, the so-called demons force. Using Gauss-Newton algorithm and an efficient second-order minimisation (ESM) scheme yields:

$$\delta\mathbf{v}(\mathbf{x}) = -\frac{R(\mathbf{x}) - T \circ \phi(\mathbf{x})}{\|J(\mathbf{x})\|^2 + \lambda_i^2/\lambda_x^2} J(\mathbf{x}) \quad (3)$$

where $J(\mathbf{x})$ is the symmetric gradient $J(\mathbf{x}) = (\nabla R(\mathbf{x}) + \nabla(T \circ \phi)(\mathbf{x}))/2$. In practice, $\delta\mathbf{v}$ is smoothed with a slight Gaussian kernel $G_{\sigma_{fl}}$ (Vercauteren et al, 2008) to ensure the resulting transformation remains diffeomorphic. This smoothing is commonly referred to as fluid-like, viscous regularisation.

In virtue of the update rule $\phi_c = \phi \circ \exp(\delta\mathbf{v}) = \exp(\mathbf{v}) \circ \exp(\delta\mathbf{v})$, we can apply the Baker-Campbell-Hausdorff (BCH) formula to estimate the correspondence velocity $\mathbf{v}_c$ without computing the logarithm of the updated correspondences ϕ_c. The BCH formula gives an approximation of the velocity field $\mathbf{v}_c = Z(\mathbf{v},\delta\mathbf{v})$ such that $\exp(\mathbf{v}_c) = \exp(\mathbf{v}) \circ \exp(\delta\mathbf{v})$. As shown in (Vercauteren et al, 2008), the first order approximation is sufficient for image registration purposes:

$$\mathbf{v}_c = Z(\mathbf{v},\delta\mathbf{v})$$
$$= \mathbf{v} + \delta\mathbf{v} + 1/2[\mathbf{v},\delta\mathbf{v}] + 1/12[\mathbf{v},[\mathbf{v},\delta\mathbf{v}]] + O(\|\delta\mathbf{v}\|^2) \quad (4)$$

In the previous equation, the Lie bracket $[\cdot,\cdot]$ is defined by $[\mathbf{v},\delta\mathbf{v}] = (\nabla\mathbf{v})\delta\mathbf{v} - (\nabla\delta\mathbf{v})\mathbf{v}$. Although it is not clear whether theoretically the space $\mathbb{G}$ is a BCH-Lie group (Glockner, 2006), BCH composition of diffeomorphisms of $\mathbb{G}$ has experimentally shown promising results in terms of image registration and statistics on diffeomorphisms (Bossa et al, 2007; Vercauteren et al, 2008).

Once $\mathbf{v}_c$ is calculated, (2) is minimised with respect to $\mathbf{v}$. In practice, this step is performed by smoothing $\mathbf{v}_c$ with a

Gaussian kernel $G_{\sigma_{el}}$. The next section investigates how σ_{el} relates to the regularisation weight λ_d. The main steps of the algorithm are reported in the pseudo-code (Algorithm 1).

Algorithm 1 LogDemons Registration

Require: Stationary velocity field $\mathbf{v}^0$. {Usually $\mathbf{v}^0 = \mathbf{0}$, i.e. $\phi^0 = \text{Id}$}.
1: **loop** {*over n until convergence*}
2:     Compute the update velocity: $\delta\mathbf{v}^n$ given $\mathbf{v}^{n-1}$ (3).
3:     Fluid-like regularisation: $\delta\mathbf{v}^n \leftarrow G_{\sigma_{fl}} \star \delta\mathbf{v}^n$, $G_{\sigma_{fl}}$ is a Gaussian kernel.
4:     Compute the correspondence velocity: $\mathbf{v}_c^n \leftarrow Z(\mathbf{v}^{n-1},\delta\mathbf{v}^n)$ (4).
5:     Diffusion-like regularisation: $\mathbf{v}^n \leftarrow G_{\sigma_{el}} \star \mathbf{v}_c^n$, $G_{\sigma_{el}}$ is a Gaussian kernel.
6:     Update the warped image $T \circ \phi^n = T \circ \exp(\mathbf{v}^n)$
7: **end loop**
8: **return** $\mathbf{v}$, $\phi = \exp(\mathbf{v})$ and $\phi^{-1} = \exp(-\mathbf{v})$.

About LogDemons Parameters LogDemons is controlled by four parameters: the image noise λ_i^2, the uncertainty on the correspondences λ_x^2 and the regularisation strengths σ_{fl}^2 and σ_{el}^2. The noise in the images is estimated at every voxel by $\lambda_i^2(\mathbf{x}) = |R(\mathbf{x}) - T \circ \phi(\mathbf{x})|^2$ (Cachier et al, 1999; Vercauteren et al, 2009). As in Thirion demons, such an estimator normalises $\delta\mathbf{v}$ to prevent too strong updates that would hamper the stability of the algorithm. In particular, building on (Cachier et al, 1999), Vercauteren et al (2009) demonstrated that the maximum amplitude of the update velocity $\delta\mathbf{v}$ is upper bounded by $\lambda_x/2$. λ_x thus controls the maximum update length per iteration. More global noise estimators fail to limit the update velocities, which can become large and ultimately yield non diffeomorphic transformations (Mansi, 2010). σ_{fl}^2 controls the strength of the fluid-like regularisation. In practice, $\sigma_{fl}^2 = 0.5$ is recommended. Finally, σ_{el}^2 controls the regularisation strength, as we shall discuss in the next section. It has to be stressed that in this article, the three parameters λ_x^2, σ_{fl}^2 and σ_{el}^2 are explicitly decoupled as in (Cachier et al, 2003; Vercauteren et al, 2008) in contrast to other formulations of demons where λ_x^2 is implicit.

3 Insights into LogDemons Regularisation: From Diffusion to Elastic-Like Regularisation

3.1 Insights into LogDemons Gaussian Regularisation

A consistent mathematical formulation of the Gaussian-based logDemons regularisation is required to adapt the algorithm to other transformation models. In scale-space theory, the diffusion equation is the Euler-Lagrange equation of a functional with L_2 image distance and Tikhonov regularisation (Nielsen et al, 1994). Now, minimising the registration energy (2) with respect to $\mathbf{v}$ amounts to minimising the regu-

larisation energy:

$$\mathscr{E}_{reg}(\mathbf{v}) = \frac{1}{\lambda_x^2} \| \log(\exp(-\mathbf{v}) \circ \exp(\mathbf{v}_c)) \|_{L_2}^2 + \frac{1}{\lambda_d^2} \| \nabla \mathbf{v} \|^2 \quad (5)$$

Linearising the first term of (5) according to the zeroth order approximation of BCH formula $(\log(\exp(-\mathbf{v}) \circ \exp(\mathbf{v}_c)) \approx \mathbf{v}_c - \mathbf{v}$ (4)) and replacing the second term with the Tikhonov regulariser enables one to formulate the logDemons regularisation as a Tikhonov problem:

$$\mathscr{E}_{reg}(\mathbf{v}) = \frac{1}{\lambda_x^2} \| \mathbf{v}_c - \mathbf{v} \|_{L_2}^2 + \int_\Omega \sum_{k=1}^{+\infty} \frac{\partial_{i_1..i_k} v_{i_{k+1}} \partial_{i_1..i_k} v_{i_{k+1}}}{\lambda_x^2 \lambda_d^{2k} k!} \quad (6)$$

This formulation will enable us to integrate more advanced regularisers. $\partial_{i_k..i_l}$ denotes the composition of the spatial derivatives $\partial_{i_k}..\partial_{i_l}$, $i_j \in [[1,d]] \, \forall j \in [[k,l]]$. v_{i_k} is the i_k^{th} component of $\mathbf{v}$. A simplified Einstein notation has been used: indices that are repeated twice in a product are summed all over their range (e.g. $v_i v_i = v_1^2 + v_2^2 + v_3^2$ if $\mathbf{v} : \mathbb{R}^3 \to \mathbb{R}^3$). The second term has been divided by λ_x^2 to simplify the calculations and the regularisation weight λ_d^2 is now function of the derivative orders to preserve the shape of the impulse response related to the regulariser (Nielsen et al, 1994).

The minimisation of (6) is classically performed in the Fourier space (Nielsen et al, 1994; Cachier and Ayache, 2004). The velocity $\mathbf{v}$ is obtained by smoothing $\mathbf{v}_c$ with the Gaussian kernel $G_{\sigma_{el}} = 1/\sqrt{2\pi\sigma_{el}^2}^d \exp(-\mathbf{x}^T\mathbf{x}/(2\sigma_{el}^2))$, with $\sigma_{el}^2 = 2/\lambda_d^2$. The demons regularisation is the exact minimiser of the regularisation energy (6). It is now clear how the width σ_{el}^2 of the Gaussian kernel relates to the strength of the regularisation λ_d^2. The higher σ_{el}^2, the lower λ_d^2 and the stronger the regularisation. It has to be noted that the derivation of (6) with respect to $\mathbf{v}$ implies that all the spatial derivatives of $\mathbf{v}$ vanish at the boundaries $\partial\Omega$ of Ω. Gaussian smoothing must be performed accordingly by extending the image periodically for instance or by ensuring that the moving structure stays far from the image boundaries.

3.2 Elastic-Like LogDemons

We can now directly integrate an elastic regularisation in the logDemons framework. To preserve demons computational efficiency, we build a regulariser based on multi-order isotropic differential quadratic forms (IDQF) whose minimiser is exactly computed using the separable elastic-like kernel filter proposed by (Cachier and Ayache, 2004). With the simplified Einstein convention, the kth-order IDQF of a vector field $\mathbf{v}$ is defined by:

$$Q_{el}^k(\mathbf{v}) = \alpha_k \partial_{i_1..i_k} v_{i_{k+1}} \partial_{i_1..i_k} v_{i_{k+1}} + \beta_k \partial_{i_1..i_k} v_{i_{k+1}} \partial_{i_{k+1} i_2..i_k} v_{i_1}$$

α_k and β_k are scalar coefficients of $\mathbb{R}$, $\alpha_k \geq 0$ and $\beta_k \geq -\alpha_k$ to ensure the positiveness of Q_{el}^k. With $\alpha_k = 1/k!$, the first

term of Q_{el}^k is the kth term of the previous Tikhonov regulariser (6). Elasticity is thus modelled by the second term of Q_{el}^k. We define the elastic regularisation as:

$$\mathscr{E}_{reg}(\mathbf{v}) = \frac{1}{\lambda_x^2} \| \mathbf{v}_c - \mathbf{v} \|_{L_2}^2 + \int_\Omega \sum_{k=1}^{+\infty} \frac{Q_{el}^k(\mathbf{v})}{\lambda_d^{2k} \lambda_x^2} \quad (7)$$

From the functional derivatives:

$$\partial_{\mathbf{v}}(\partial_{i_1..i_k} \mathbf{v}_{i_{k+1}} \partial_{i_1..i_k} \mathbf{v}_{i_{k+1}}) = (-1)^k \Delta^k \mathbf{v}$$
$$\partial_{\mathbf{v}}(\partial_{i_1..i_k} \mathbf{v}_{i_{k+1}} \partial_{i_{k+1} i_2..i_k} \mathbf{v}_{i_1}) = (-1)^k \Delta^{k-1} \nabla\nabla^T \mathbf{v}$$

it follows the optimal condition:

$$\mathbf{v} + \sum_{k=1}^\infty \frac{(-1)^k}{\lambda_d^{2k}} \left[\alpha_k \triangle^k \mathbf{v} + \beta_k \triangle^{k-1} \nabla\nabla^T \mathbf{v} \right] = \mathbf{v}_c \quad (8)$$

which is solved in the Fourier domain. Note that when $k = 1$, the energy becomes the first-order Lamé elastic equation. Let $\hat{\mathbf{v}}(\mathbf{w}) = \mathfrak{F}(\mathbf{v}(\mathbf{x}))$ be the Fourier transform of the velocity field $\mathbf{v}(\mathbf{x})$, $\mathbf{w}$ is the frequency variable. According to the identities

$$\mathfrak{F}\left(\triangle^k \mathbf{v}(\mathbf{x})\right) = (-1)^k \left(\mathbf{w}^T\mathbf{w}\right)^k \hat{\mathbf{v}}(\mathbf{w})$$
$$\mathfrak{F}(\triangle^{k-1} \nabla\nabla^T \mathbf{v}(\mathbf{x})) = (-1)^k (\mathbf{w}^T\mathbf{w})^{k-1} \mathbf{w}\mathbf{w}^T \hat{\mathbf{v}}(\mathbf{w})$$

(8) is transformed as:

$$\left[\underbrace{\left(1 + \sum_{k=1}^\infty \frac{\alpha_k(\mathbf{w}^T\mathbf{w})^k}{\lambda_d^{2k}}\right)}_{A} \mathrm{Id} + \underbrace{\left(\sum_{k=1}^\infty \frac{\beta_k(\mathbf{w}^T\mathbf{w})^{k-1}}{\lambda_d^{2k}}\right)}_{B} \mathbf{w}\mathbf{w}^T \right] \hat{\mathbf{v}}(\mathbf{w}) = \hat{\mathbf{v}}_c(\mathbf{w})$$

Since A and B are scalars, we can apply Sherman-Morrison inversion formula, which yields the closed form solution:

$$\hat{\mathbf{v}}(\mathbf{w}) = \underbrace{\left[\frac{1}{A}\mathrm{Id} - \frac{1}{A}\left(\frac{B}{A + B\mathbf{w}^T\mathbf{w}}\right)\mathbf{w}\mathbf{w}^T\right]}_{M} \hat{\mathbf{v}}_c(\mathbf{w})$$

The optimal velocity field $\mathbf{v}$ is therefore obtained by filtering in the Fourier domain the correspondence velocity $\mathbf{v}_c$ with the filter M. Computational efficiency can be greatly improved by choosing the coefficients α_k and β_k such that M is separable. If $\alpha_k = 1/k!$, A is the Gaussian kernel found in the previous section. One can demonstrate (see Appendix B) that if β_k is defined by $\beta_0 = 0$, $\beta_k = \sum_{i=1}^k \gamma^i \lambda_d^{2i}/(k-i)! \, \forall k \geq 1$ and $\gamma \in \mathbb{R}$, then the second term of the filter M is proportional to the Hessian of the Gaussian kernel $\exp(\mathbf{w}^T\mathbf{w}/\lambda_d^2)$. With $\sigma_{el}^2 = 2/\lambda_d^2$ and $\gamma = \sigma_{el}^2 \kappa/(\kappa+1)$ we retrieve the elastic-like separable vector filter proposed by Cachier and Ayache (2004):

$$\mathbf{v} = \left(G_{\sigma_{el}} \mathrm{Id} + \frac{\sigma_{el}^2 \kappa}{1 + \kappa} \mathscr{H} G_{\sigma_{el}}\right) \star \mathbf{v}_c = G_{\sigma_{el},\kappa} \star \mathbf{v}_c \quad (9)$$

$\mathscr{H}G_{\sigma_{el}}(\mathbf{x})$ is the Hessian of the Gaussian kernel $G_{\sigma_{el}}$ and $G_{\sigma_{el},\kappa}$ is the elastic-like vector filter. When $\kappa = 0$, $G_{\sigma_{el},\kappa=0}$ is the Gaussian filter and the elastic regularisation energy (7) is exactly the diffusion energy (6). It is therefore straightforward to switch the regulariser.

As for the diffusion regularisation, σ_{el}^2 controls the strength of the regularisation. The *elastic* parameter κ behaves like the Poisson ratio ν of the theory of elasticity by controlling the cross-effects of the smoothing between the vector components. Cachier and Ayache (2004) showed that the higher κ, the more incompressible the deformation. This property still holds here even though $G_{\sigma_{el},\kappa}$ acts on velocities and not on deformations. The stationary velocities $\mathbf{v}$ are parameters of the deformations, their norm is directly related to the length of the deformations through $\int_0^1 \|\mathbf{v}(t)\|_V^2 dt^{1/2} = \|\mathbf{v}(t=0)\|_V^2$, where V is the space of velocities. Smoothing $\mathbf{v}(t=0)$ thus amounts to smoothing ϕ. This is very different from fluid registration which regularises the infinitesimal increments i.e., the instant velocities $\mathbf{v}(t)$.

Elastic-like regularisation may not be sufficient to recover locally incompressible deformations. κ only controls incompressibility at a global scale as it is a global parameter. Furthermore, perfect incompressibility would be reached only when $\kappa \to \infty$. As a result, hard constraints must be used when strong incompressibility is required.

4 Incompressible LogDemons

A transformation ϕ is locally incompressible if its Jacobian determinant $|\nabla\phi|$ equals one. This non-linear constraint however is computationally demanding. For diffeomorphic transformations one can show that the condition on fluid motion holds: Integrating divergence-free velocities over time yields incompressible deformations (Evans, 1998). Making logDemons incompressible is thus achieved by constraining the velocity field $\mathbf{v}$ to be divergence-free. This only alters the regularisation step as the optimisation stage optimises $\mathscr{E}(\mathbf{v},\mathbf{v}_c)$ with respect to the correspondence velocity $\mathbf{v}_c$.

Helmholtz decomposition states that any velocity $\mathbf{v}$ that vanishes at infinity can be uniquely decomposed in the sum of a divergence-free field and a curl-free field. Using variational calculus and Lagrangian multipliers, Simard and Mailloux (1988) demonstrated that the Helmholtz decomposition projects $\mathbf{v}$ onto the space of divergence-free vector field in the L_2-norm sense. In this work, we employ a similar technique to constrain the registration to be divergence-free. We want to minimise (7) under the constraint $\nabla \cdot \mathbf{v} = 0$. Let p be the Lagrangian multiplier associated to that constraint. p is a scalar field with compact support Ω. Minimisers of (7) (or (6) if $\kappa = 0$) under the divergence-free constraint are op-

tima of the Lagrange function:

$$\mathscr{P}_{reg}(\mathbf{v},p) = \frac{1}{\lambda_x^2}\|\mathbf{v}_c - \mathbf{v}\|_{L_2}^2 + \int_\Omega \sum_{k=1}^{+\infty} \frac{Q_{el}^k}{\lambda_x^2 \lambda_d^{2k}} - \frac{2}{\lambda_x^2}\int_\Omega p\,\nabla\cdot\mathbf{v} \tag{10}$$

Calculating the Gâteaux derivatives of (10) yields the two optimal conditions:

$$\nabla \cdot \mathbf{v} = 0 \tag{11}$$

$$\mathbf{v} + \sum_{k=1}^\infty \frac{(-1)^k}{\lambda_d^{2k}}(\alpha_k \triangle^k \mathbf{v} + \beta_k \triangle^{k-1}\nabla\nabla^T\mathbf{v}) = \mathbf{v}_c - \nabla p \tag{12}$$

with $p = 0$ at the boundaries $\partial\Omega$ of the image domain. The optimal velocity field $\mathbf{v}$ is therefore computed by smoothing the right hand side of the previous equation, $\mathbf{g} = \mathbf{v}_c - \nabla p$, with the kernel $G_{\sigma_{el},\kappa}$. To compute $\mathbf{g}$, we take the divergence of (12) under the optimal condition $\nabla \cdot \mathbf{v} = 0$. This yields the Poisson equation under 0-Dirichlet boundary conditions:

$$\triangle p = \nabla \cdot \mathbf{v}_c \tag{13}$$

p can thus be computed independently of $\mathbf{v}$ by solving (13). This is exactly the Helmholtz decomposition of $\mathbf{v}_c$. $\mathbf{g} = \mathbf{v}_c - \nabla p$ is the L_2 projection of $\mathbf{v}_c$ to the space of divergence-free vector fields, as $\nabla \cdot \mathbf{g} = \nabla \cdot \mathbf{v}_c - \triangle p = 0$. ∇p is the orthogonal curl-free component. Ensuring divergence-free velocity fields thus consists in *i)* projecting the correspondence velocity onto the space of divergence-free vector fields and *ii)* smoothing the result.

With this approach, the incompressibility constraint can be applied within a subdomain $\Gamma \subset \Omega$ by defining $p \in H_0^1(\Gamma)$, $p = 0$ on Ω/Γ. This may be useful for tracking incompressible tissues localised in space, like the cardiac muscle. However, particular care must be taken at the domain boundaries $\partial\Gamma$. Although Gaussian smoothing theoretically preserves vector field divergence, in practice unconstrained velocities close to $\partial\Gamma$ may leak inside the incompressible domain due to the Gaussian convolution, ultimately resulting in volume drifts. Yet, Gaussian filter and vector derivatives commute for well-designed filters such as Deriche recursive filters (Deriche, 1993). We therefore replace the theoretical "project-and-smooth" strategy by a "smooth-and-project" approach that preserves the divergence close to $\partial\Gamma$. To further limit numerical instabilities, a smooth domain transition is implemented in a narrow band around Γ by diffusing the pressure field p using the heat-transfer equation (Evans, 1998). The main steps of the proposed algorithm, henceforth termed *iLogDemons*, are summarised in (Algorithm 2). Note that incompressibility can be easily disabled by skipping the steps 6 and 7 of the algorithm.

Algorithm 2 iLogDemons: Incompressible Elastic-Like LogDemons Registration

---

Require: Stationary velocity field $\mathbf{v}^0$. {Usually $\mathbf{v}^0 = \mathbf{0}$ i.e. $\phi^0 = \text{Id}$}.
 1: **loop** {*over n until convergence*}
 2:    Compute the update velocity: $\delta\mathbf{v}^n$ given $\mathbf{v}^{n-1}$ (3).
 3:    Fluid-like regularisation: $\delta\mathbf{v}^n \leftarrow G_{\sigma_{fl}} \star \delta\mathbf{v}^n$, $G_{\sigma_{fl}}$ is a Gaussian kernel.
 4:    Compute the correspondence velocity: $\mathbf{v}_c^n \leftarrow Z(\mathbf{v}^{n-1}, \delta\mathbf{v}^n)$ (4).
 5:    Elastic-like regularisation: $\mathbf{v}^n \leftarrow G_{\sigma_{el},\kappa} \star \mathbf{v}_c^n$ (9)
 6:    Solve: $\Delta p = \nabla \cdot \mathbf{v}^n$ with 0-Dirichlet boundary conditions (13)
 7:    Project the velocity field: $\mathbf{v}^n \leftarrow \mathbf{v}^n - \nabla p$.
 8:    Update the warped image $T \circ \phi^n = T \circ \exp(\mathbf{v}^n)$
 9: **end loop**
10: **return** $\mathbf{v}$, $\phi = \exp(\mathbf{v})$ and $\phi^{-1} = \exp(-\mathbf{v})$.

About the Divergence-Free Update Velocity One could also constrain the correspondence field ϕ_c to be incompressible in order to find the optimal image matching that satisfies the constraint (see Appendix C). When the transformation ϕ is incompressible, it follows from the diffeomorphic update rule $\phi_c \leftarrow \phi \circ \exp(\delta\mathbf{v})$ that ϕ_c is incompressible if $\delta\mathbf{v}$ is divergence-free. Yet, from a theoretical perspective, adding such a constraint to the iLogDemons would have little effect on the result. In theory, constraining $\mathbf{v}$ to be divergence-free amounts to projecting $\mathbf{v}_c$ to the space of divergence-free vector fields. ϕ_c is therefore incompressible. Since the composition of two continuous incompressible fields is incompressible, $\exp(\delta\mathbf{v})$ is also incompressible and $\delta\mathbf{v}$ is divergence-free. When the zeroth order BCH approximation is used to compute $\mathbf{v}_c$, the linearity of the projector yields the same conclusion. The two approaches are hence equivalent. Nonetheless, small differences may arise in practice due to the numerical approximations (scaling-and-squaring, numerical accuracy of the composition, etc.) We will experimentally evaluate when it is necessary to add such a constraint.

Numerical Implementation The algorithm was implemented in ITK from the open source implementation of the log-Demons (Dru and Vercauteren, 2009). The Poisson equation (13) is solved using finite differences on the regular image grid (Simard and Mailloux (1988), PETSc library). Contrary to Fourier-based techniques (Hinkle et al, 2009), the direct resolution can be performed on an incompressible domain Γ of arbitrary shape by rasterising it on the image grid. More sophisticated finite elements approaches could also be used. Image gradients are computed with periodic boundary conditions (Dru and Vercauteren, 2009) and the Gaussian filters are implemented with ITK recursive filters (Deriche, 1993).

5 Experiments and Results

Three experiments were performed to evaluate how much iLogDemons improves the recovery of incompressible deformations with respect to the original logDemons.

1. We first tested on synthetic datasets the ability of the elastic regularisation alone to estimate random incompressible deformations.
2. We then tested extensively the incompressibility constraint on large analytic incompressible transformations to quantify the improvements with respect to logDemons.
3. We finally applied the iLogDemons to estimate left ventricular myocardium motion from multi-slice short axis cine magnetic resonance images (cMRI). The results were compared with logDemons using tagged MRI (tMRI) measurements as reference.

In the following, *logDemons* refers to the unconstrained logDemons algorithm, either with diffusion or elastic-like regularisation (Algorithm 1). *iLogDemons* refers to the proposed incompressible logDemons algorithm, where the velocities $\mathbf{v}$ are constrained to be divergence-free (Algorithm 2). We also evaluated the fully constrained iLogDemons, where both the update velocities $\delta\mathbf{v}$ and the velocity $\mathbf{v}$ are divergence-free. This algorithm is called $i^2 LogDemons$. The software developed for these experiments will be available at http://www-sop.inria.fr/asclepios/software.php.

5.1 Global Incompressibility Recovery Using Elastic Regularisation

As we have seen, elastic regulariser theoretically provides more incompressible deformation fields, controlled by the global parameter κ. Here, we experimentally test how much this feature alone (no incompressibility constraint) can help in recovering random incompressible deformation fields.

5.1.1 Illustration on Translated Cubes

We first tested the elastic-like regularisation on a toy example to have an intuition of the results. Two translated black-and-white small cubes were co-registered using the diffusion ($\sigma_{el}^2 = 1, \kappa = 0$) and the elastic-like ($\sigma_{el}^2 = 1$, $\kappa = 0.5$ and $\kappa = 100$) regularisation. As illustrated in Fig. 1, the elastic-like regularisation yielded deformations globally more incompressible as it distributed the smoothing across the deformation components, thus reducing the compressions around the cube. We also observed that increasing κ yielded deformations closer to the true translation by better preserving the volume. Although this may not seem as accurate as with the linear elastic energy, the proposed regulariser prevents overlaps and ensures smooth spatial derivatives of the transformations, which is of particular importance when estimating the myocardium strain for instance.
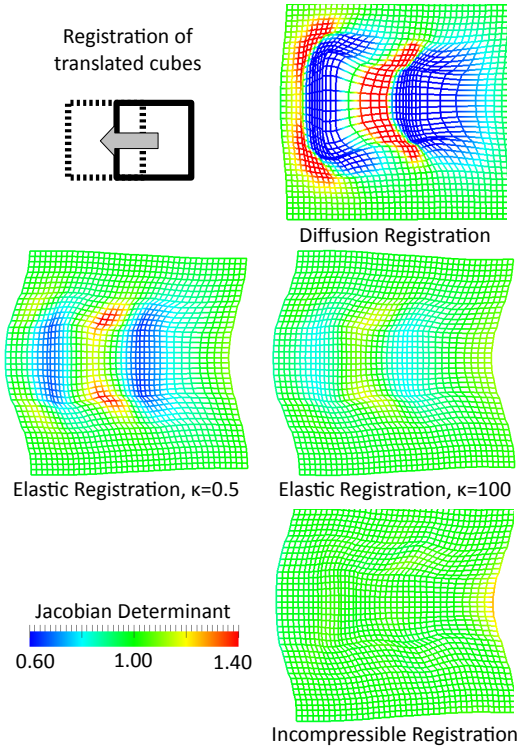
Fig. 1 Registration of two translated cubes using diffusion log-Demons, elastic-like logDemons and iLogDemons. At similar grey level RMSE, elastic-like regularisation yielded stiffer deformations (the higher κ, the stiffer) but only iLogDemons provided an incompressible deformation close to the true translation.

5.1.2 Quantitative Evaluation on Random Incompressible Deformations

The impact of the elastic-like regularisation on the estimation of incompressible deformations was quantified on synthetic data sets generated as follows. A 3D isotropic Steady-State Free Precession (SSFP) MR image of the heart ($53 \times 60 \times 60$ slices, $1\,mm^3$ voxel spacing), henceforth called test image, was warped by 50 random incompressible deformation fields. Warped and test images were then altered with a slight Gaussian noise (SD= 3, range of grey level intensities: $[0:198]$) (Fig. 2**A-B**).

The random deformation fields were generated by integrating divergence-free velocity fields. Each voxel was assigned a random velocity according to a Gaussian distribution with high standard deviation to get large displacements and large strains (SD= $5000\,mm/s$). The resulting velocity field was smoothed with a Gaussian kernel (SD= $3\,mm$) and its L_2-norm was normalised to $2\,mm$. We then made it divergence-free using Helmholtz decomposition and integrated the result with the "scaling-and-squaring" algorithm (Appendix A) to get the final incompressible deformation (Fig. 2**C**). The average L_2-norm of the deformation fields was $1.83 \pm 0.77\,mm$ (mean $\pm$ standard deviation SD). Their Jacobian determinant was very close to the incompressibil-

ity condition $|\nabla\phi| = 1$ (0.99 ± 0.03, Fig. 2**D**). We verified with this procedure that "scaling-and-squaring" divergence free velocity fields do yield near incompressible deformations. Indeed, directly integrating the original non divergence-free velocities yielded deformations with similar L_2-norm ($1.91 \pm 0.99\,mm$) but that did not preserve volume ($|\nabla\phi| = 1 \pm 0.53$)
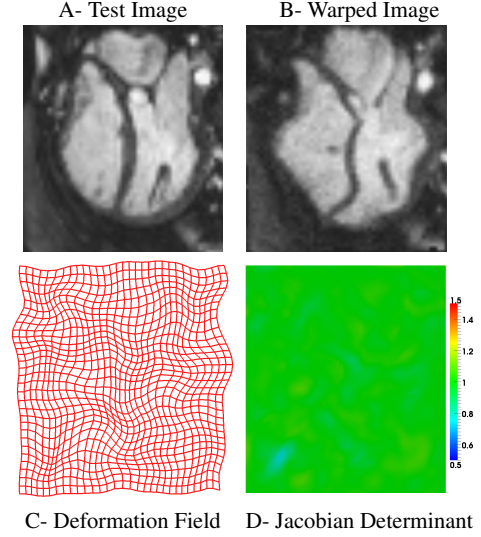

Fig. 2 Synthetic 3D image warped with a random incompressible deformation field (represented by a warped grid).

We registered the 50 warped images to the test image with and without elastic regularisation. The following registration parameters were used, $\sigma_{fl}^2 = 1$, $\sigma_{el}^2 = 1$ and $\lambda_x = 1$, and no multi-resolution scheme was used as we aimed at comparing two methods rather than pure performance. The number of demons iterations was fixed to 50. Several elastic parameter values were tested: $\kappa = \{0, 0.1, 0.5, 1, 2, 10, 100\}$. Registration accuracy was measured using the distance to the true deformation field (DTF) and the relative mean squared error of image intensities (RMSE) defined by:

$$\mathrm{DTF}(\phi, \phi_{ref}) = \|\phi - \phi_{ref}\|_{L_2}$$
$$\mathrm{RMSE}(T, R \circ \phi) = \|T - R \circ \phi\|^2 / \|T - R\|^2$$

For both indices, the lower the value, the better. Variations in registration performances were quantified using the coefficients of variation $\nu = sd/mean$ of RMSE, DTF and Jacobian determinant. Low ν values mean little impact of the elastic regularisation on a particular metric.

The results showed that deformation field recovery and image matching accuracy did not change significantly by increasing κ ($\nu_{\mathrm{DTF}} \approx 1.6\%$, $\nu_{\mathrm{RMSE}} \approx 8.5\%$, Fig. 3). However, increasing κ largely reduced the standard deviation of the Jacobian determinant ($\nu_{\mathrm{std(Jac.)}} \approx 36\%$) while its mean was close to one ($\nu_{\mathrm{mean(Jac.)}} \approx 0.18\%$). The elastic regularisation

thus improved global incompressibility of the deformation, as observed in the toy example (Fig. 1), but it did not change the local accuracy of the registration. A strong constraint is needed to recover locally incompressible deformations.
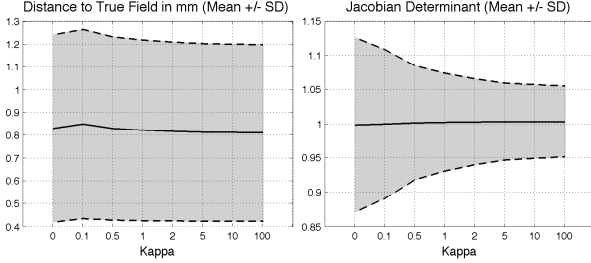

Fig. 3 Effect of elastic-like regularisation on registration performances. These curves show that elastic-like regularisation, controlled by the parameter κ, does not affect registration accuracy (low variation of distance to true field, *left panel*) while it significantly decreases Jacobian determinant standard deviation (*right panel*). The deformation is globally more incompressible.

5.2 Local Incompressibility Recovery Using Volume-Preserving Constraint

We now evaluate how much the incompressibility constraint, without elastic regularisation, can recover locally but strong volume-preserving deformation fields.

5.2.1 Illustration on Translated Cubes

As for the elastic regularisation, we first tested the incompressibility constraint on the small cubes to get an intuition of the results. Elastic regularisation was disabled ($\sigma_{el}^2 = 1$, $\kappa = 0$) and the incompressibility constraint was enabled. As one can see in Fig. 1, the incompressibility constraint prevented the compressions around the cubes. The recovered translation was qualitatively better than the displacements estimated using the diffusion and the elastic registration methods.

5.2.2 Quantitative Evaluation on Analytic Incompressible Whirls

We quantified the previous qualitative observation on synthetic data generated by warping the test image with analytic whirl transformations (Fig. 4). We decided not to use the previous synthetic dataset to avoid any bias as the deformations were generated using divergence free velocities, like the proposed constraint. Furthermore, analytic whirls enable to work on much larger but still volume-preserving deformations.

Eight volume preserving whirl transformations were created as in (Saddi et al, 2007). The voxel O at the centre of the image domain was the centre of the whirl. All the voxels P that were outside the sphere of radius R and centred in O did not move. The voxels P inside the sphere were rotated with respect to O with an angle $\alpha(P) = \alpha_0(1 - \text{dist}(P, O)/R)^2$. The strength of the deformation was controlled by the whirl angle α_0, spanning from $10°$ to $80°$. Within the whirl domain, the L_2-norm varied from $0.52\,mm$ to $4.78\,mm$ but the Jacobian determinant remained close to one (worst value: $|\phi_{\alpha_0=80°}| = 1 \pm 0.04$).
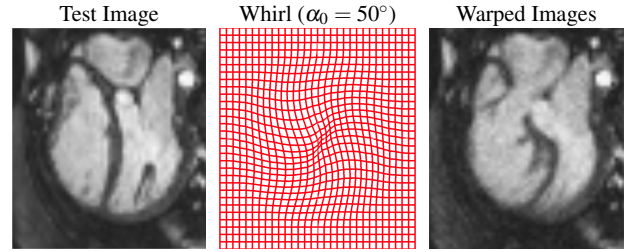

Fig. 4 Synthetic 3D image warped with an analytic whirl transformation (represented by a warped grid).

The 8 images T warped using the whirl transformations ϕ_{α_0} were registered to the test image R using LogDemons and iLogDemons ($\lambda_x = 1$, $\sigma_{el}^2 = 1$, $\sigma_{fl}^2 = 1$, $\kappa = 0$, number of iterations fixed to 150 to ensure convergence at any whirl angle). RMSE, Jacobian determinant and DTF are reported in Fig. 5. As expected, the deformation fields estimated with iLogDemons were almost incompressible. Jacobian determinants were always equal to 1 ± 0.02 independently of the strength of the whirl to recover. Image matching accuracy was not affected by the incompressibility constraint, showing only 0.6% decrease. The higher RMSE at small whirl angles is due to the relative nature of that metric. In those cases, the images are already fairly close to each other and slight image matching errors yield larger RMSE. Most importantly, iLogDemons significantly improved the accuracy of the recovered deformation fields. Means and standard deviations of DTF were systematically lower (average improvements of 29% and 36% respectively). The larger the deformation, the more significant the improvement while RMSE stayed comparable. This experiment demonstrated the importance of the transformation model. As illustrated in Fig. 6, regions with homogeneous grey levels provided few information to accurately estimate the whirl. With the iLogDemons, the incompressibility constraint helped the algorithm by ensuring that the estimated deformation is of the same type as the true field. This feature is particularly interesting for clinical applications, where deformations must be reliably estimated from ill-textured images. In particular, we observed than iLogDemons provided significantly more

accurate results that the original algorithm in images with very large slice thicknesses (see Appendix D for results on synthetic data).
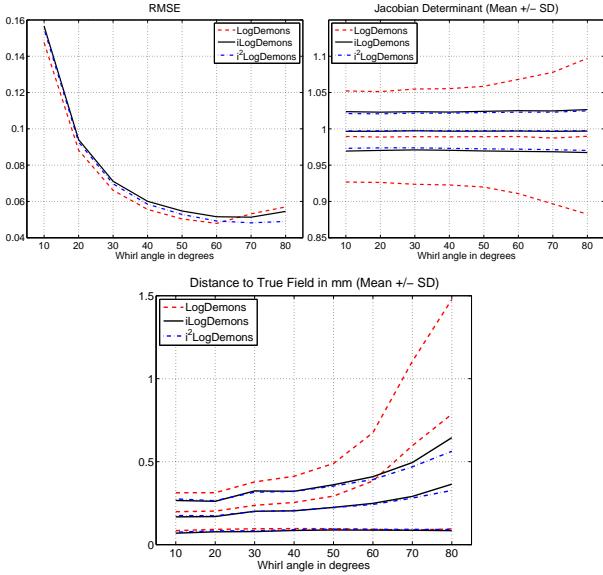

Fig. 5 Results of the registration of whirl datasets. With similar image matching performances (similar RMSE of image intensities, *top-left panel*), iLogDemons provided more incompressible deformations (Jacobian determinant closer to one, *top-right panel*, mean $\pm$ SD are displayed) and outperformed LogDemons in terms of deformation field accuracy (lower DTF, *bottom panel*, mean $\pm$ SD are displayed). Constraining the update velocity to be divergence-free (i^{2}LogDemons) did not improve the results significantly.

We also investigated whether the performances were improved using i^{2}LogDemons, which also enforces the update velocity field to be divergence-free (Appendix C). Results, reported in Fig. 5, were in agreement with the theoretical considerations (Sec. 4). Relevant differences only appeared at large deformations ($\alpha_0 \geq 70°$). Finally, it should be noted that all these observations continue to hold with $\lambda_x = 2, 4$ and on random incompressible fields (experiments not reported here), supporting robustness to parameters.

To conclude, the experiments on synthetic data showed that i) elastic regularisation provides deformation fields with better global incompressibility but does not significantly improve the local accuracy of the registration; ii) the proposed incompressibility constraint provides almost incompressible deformations and improves the recovery of volume preserving deformations. Both contributions are therefore complementary and can be used jointly to obtain smooth, globally and locally incompressible deformation fields. In the next section we evaluate the proposed algorithm in a concrete clinical application.
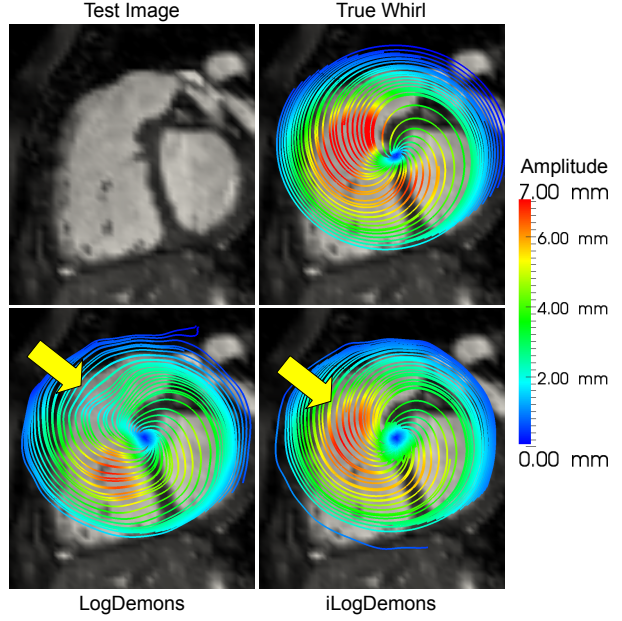

Fig. 6 Streamlines of true and estimated whirl deformations (whirl angle $\alpha_0 = 60°$). Colours encode deformation amplitude in mm. iLog-Demons better estimated the whirl transformation in regions with poor texture (*yellow arrow*), providing more accurate motion and deformation amplitude.

5.3 Application to Cardiac Deformation Recovery

As a feasibility study, we applied iLogDemons to estimate the 3D strain of the left-ventricular cardiac muscle, the myocardium, from standard anatomical cine MR images (cMRI) of the heart (Fig. 7). Widely available in clinical routine, these images have good in-plane and temporal resolutions. However, they only show the apparent motion of the heart as no texture is present within the myocardium. Combined with their large slice thickness, accurate estimation of cardiac motion from cMRI is challenging. During the cardiac cycle, it has been reported that the volume of the heart muscle does not vary significantly ($\approx 5\%$ of volume variation (Glass et al, 1991)). It is therefore reasonable to use incompressibility constraints to estimate cardiac motion (Bistoquet et al, 2008). We thus applied iLogDemons to estimate the 3D myocardium strain on cMRI of two adult patients with heart failure. Results were compared with those obtained using logDemons and the ground truth provided by tagged MRI.

Image Acquisition and Preparation Anatomical cMRI were acquired in the short axis view with multiple breath-holds (Achieva, Philips Medical System, 30 time frames, $1.4\,mm^2$ isotropic in-plane resolution, $10\,mm$ slice thickness). For the first patient, 3D tagged MR images (tMRI) were acquired during the same exam (CSPAMM encoding, 23 time frames, $1.0\,mm^3$ isotropic resolution, tag size $\approx 7\,mm$, Fig. 9 left panel). No manual tracking of the tag grids was available
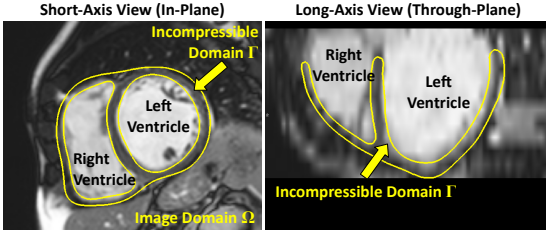
Fig. 7 Short-axis cine-MRI of patient 1. Incompressibility is ensured only within the myocardium (outlined in yellow). Note the lack of consistent texture within the myocardium even in the in-plane image (*left panel*) and the coarse through plane resolution (*right panel*).

as this task is extremely difficult due to the 3D nature of the motion. For the second patient, 2D tMRI were acquired in the short axis view (23 time frames, $1.1\,mm^2$ in-plane resolution, $18\,mm$ slice thickness, tag size $\approx 6\,mm$). For this case, manual tracking of the tag grids was performed by an expert in the short axis view. All images fully covered both ventricles. The two cMRI and the 3D tMRI presented no slice misalignments. The tMRI were spatially and temporally aligned to the cMRI using DICOM information. Finally, the dense transformations were defined on an isotropic sampling grid adjusted to the image dimensions to cope with the large slice thickness that can introduce high frequencies in the transformations, resulting in numerical instabilities and lower registration accuracy. In practice, this amounts to linearly resampling the cMRI to get isotropic voxels.

Tracking Protocol Because the transformations provided by demons algorithm are resampling fields, myocardium motion was estimated by recursively registering all the frames of the cardiac sequence to the end-diastole (ED) time frame as in (Mansi et al, 2009) (Fig. 8), when the heart is at rest position. Registration parameters were fixed: $\lambda_x = 1$, $\sigma_{el}^2 = 2$, $\sigma_{fl}^2 = 0.5$. A 2-level multi-resolution scheme was used and registration was stopped as soon as RMSE stopped decreasing. For iLogDemons, elastic regularisation ($\kappa = 1$) was applied everywhere in the images whereas the incompressibility constraint was applied only within the myocardium as the volume of surrounding structures like blood pools vary (Fig. 7). Thanks to the backward strategy, myocardium region had to be defined only at the ED time frame. Finally, the 3D displacements and strains were projected onto the radial, circumferential and longitudinal directions as defined in (Moore et al, 2000) (Fig. 9, right panel). Strains were computed using the 3D Lagrangian finite strain tensor $\mathbf{E}(\mathbf{x}) = \frac{1}{2}\left[\nabla\mathbf{u}(\mathbf{x}) + \nabla\mathbf{u}^T(\mathbf{x}) + \nabla\mathbf{u}^T(\mathbf{x})\nabla\mathbf{u}(\mathbf{x})\right]$, where $\mathbf{u}(\mathbf{x})$ is the displacement at $\mathbf{x}$.

Comparison with 3D tMRI In a first stage, we estimated the cardiac motion of patient 1 by tracking the heart in the 3D tMRI using both iLogDemons and logDemons. We verified that iLogDemons preserved the volume of the myocardium
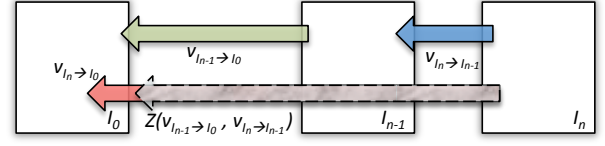

Fig. 8 Recursive tracking algorithm. Knowing the velocity $\mathbf{v}_{I_{n-1}\to I_0}$ (*green*): 1) Estimate $\mathbf{v}_{I_n\to I_{n-1}}$ (*blue*). 2) Concatenate $\mathbf{v}_{I_n\to I_{n-1}}$ and $\mathbf{v}_{I_{n-1}\to I_0}$ (*grey*) using BCH formula (4). 3) Estimate $\mathbf{v}_{I_n\to I_0}$ using 2) as initialisation (*red*).
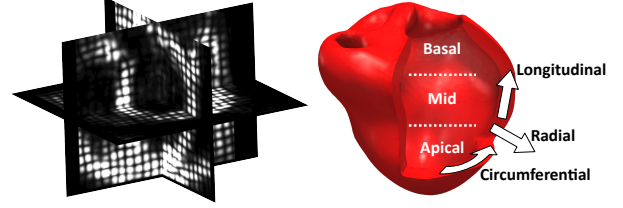

Fig. 9 *Left panel*: 3D tMRI of patient 1. *Right panel*: Definition of cardiac motion directions and heart regions.

below the values reported in the literature during the entire cardiac cycle (average volume variation: 2%, max.: 6%) contrary to logDemons (average volume variation: 26%, max.: 32%) (Fig. 10). We also observed that the incompressibility constraint reduced the deviations of the estimated displacements throughout the cardiac cycle despite the simple tracking procedure.

For visual assessment, we applied the estimated deformations to virtual planes manually positioned at ED (Fig. 11). Realistic deformations consistent with the tag grids were obtained with both algorithms. The similar performances between logDemons and iLogDemons, quantified by the low L_2-distance between recovered deformation fields (Table 1), is justified by the fact that the tag grids provided enough texture information within the myocardium to guide the registration. As no ground truth was available, we considered the displacements estimated on the 3D tMRI using iLogDemons as reference.

Table 1 L_2-distances averaged over the cardiac cycle between estimated displacements. Values to be compared with the tag size ($6mm$). Tracking cardiac motion on tMRI with logDemons and iLogDemons yielded globally small differences. When tracking the heart on cMRI, iLogDemons improved the results, the incompressibility constraint coped with the lack of myocardial texture and the large slice thickness.

Method	L_2-distance (mean $\pm$ sd, max)
iLogDemons (*tMRI*)	reference
logDemons (*tMRI*)	$1.7 \pm 0.71mm, 3.2mm$
logDemons (*cMRI*)	$3.2 \pm 0.92mm, 4.6mm$
ilogDemons (*cMRI*)	$2.8 \pm 0.72mm, 4.0mm$

We then estimated the 3D motion of the heart from the cMRI and compared the results with the reference tMRI deformation. Visual assessment of the warped virtual planes
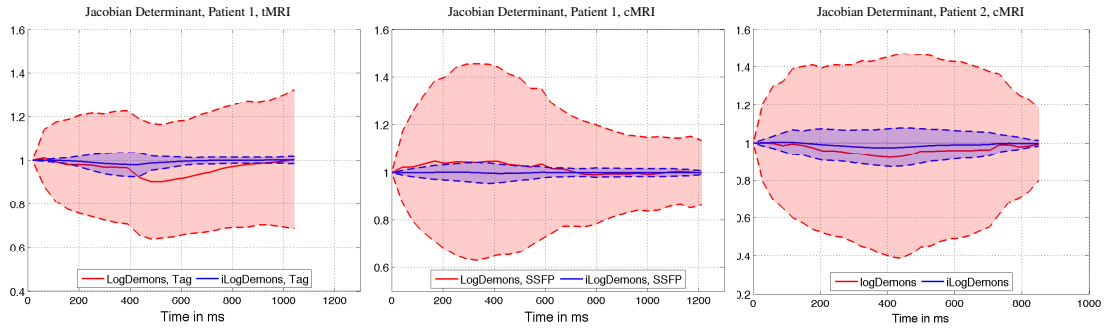
Fig. 10 Jacobian Determinant of Myocardium Motion. Curves represent mean (plain lines)± standard deviation (dashed lines). Incompressibility constraint significantly decreased volume variations during the cardiac cycle. One can observe that the constraint also controlled the volume deviation at the end of the cycle.
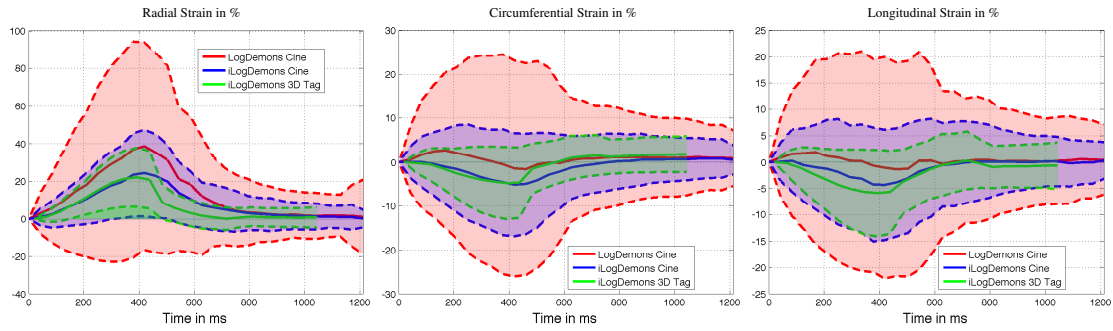

Fig. 12 Myocardium strains computed from cMRI and 3D tMRI of patient 1. Mean and standard deviation computed over the entire left ventricle. iLogDemons better estimated circumferential and longitudinal strains despite the lack of image information and the large slice thickness.

showed that the incompressibility constraint did help in recovering longitudinal and circumferential displacements despite the large slice thickness and the lack of texture features within the myocardium (Fig. 11, blue and red curves, Table 1). Estimated longitudinal and circumferential strains confirmed this finding (Fig. 12). Values obtained using iLogDemons were much closer to the reference (86% of improvement for the radial strain, 89% for the circumferential strain and 64% for the longitudinal strain). The amplitude of the radial strain was more plausible and the temporal variation patterns of the circumferential and longitudinal strains were consistent with the clinical literature (Moore et al, 2000). Note that logDemons exhibited an incorrect lengthening in both longitudinal and circumferential directions at the beginning of the cardiac contraction. Furthermore, the variability in strain measurements is significantly reduced using iLogDemons, which suggests that the estimated motion is globally more consistent.

Comparison with Manual Tracking We then estimated the cardiac motion of the second patient using logDemons and iLogDemons on cMRI and compared the results with manual tracking of 2D tag grids. As with the previous patient, iLogDemons controlled myocardium volume variations all along the cardiac cycle compared to logDemons (average
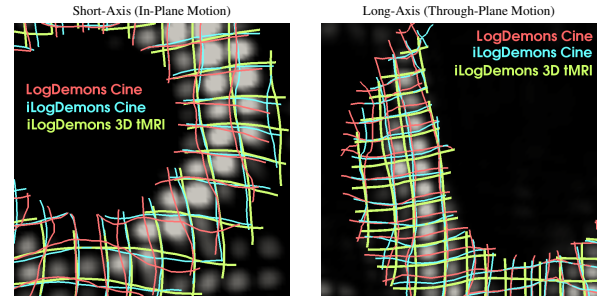

Fig. 11 Close-up of the tMRI of patient 1 at end-systole. The virtual tag planes were warped with the deformation estimated on the tMRI using iLogDemons (*green*) and with those estimated on the cMRI using logDemons (*red*) and iLogDemons (*blue*). The green planes show that the motion estimated on tMRI using iLogDemons was similar to the MRI tags. From the blue and red planes one can see that iLogDemons better estimated myocardium motion even in cMRI.

volume variation: 7%, max.: 10%, and 42%, max.: 54% respectively, Fig. 10). Point-wise motion comparison between cMRI and manual tracking was not possible due to a non-perfect tMRI-to-cMRI alignment because of tMRI slice misalignment and patient motion between scans. We thus compared the regional displacements averaged over 12 heart zones (6 basal and 6 mid-ventricular regions). Note that the slice misalignments of the tMRI did not affect the evaluation as

the measurements were exclusively 2D. For fair comparison, we transformed the 3D displacements estimated from the cMRI to apparent 2D displacements by warping the short-axis displacement (XY-plane) along the through plane motion (Z-direction). The results showed that iLogDemons, in this patient, improved the accuracy of the recovered motion. The amplitude of the radial displacement was closer to the ground truth (global error with respect to tag displacements from $2.4 \pm 2.4mm$ to $1.2 \pm 1.6mm$, about the voxel size, Fig. 13). Note that logDemons already estimated realistic radial motion patterns, yet over-estimated, as the apparent cardiac displacements in cMRI are radial to the LV boundaries. The circumferential motion provided by iLog-Demons was more realistic than the one estimated using log-Demons, yet still under-estimated (global error from $2.3 \pm 1.7mm$ to $3.5 \pm 2.0mm$, Fig. 14). The sign and dynamics of the average circumferential displacement were correctly recovered for every region except for regions 8 and 12, whereas logDemons failed to estimate the circumferential motion of most of the regions (arrows A and B in Fig. 14). The incompressibility constraint assisted the registration algorithm by redistributing the apparent radial displacement across the other direction to preserve myocardium volume.

Computation Time For the first patient, the frame-by-frame registration took $129s$ with logDemons ($4.8s$ per iterations), $296s$ with iLogDemons ($10.9s$ per iterations) and $1311s$ with i^2LogDemons ($48.6s$ per iterations) on a MacPro 2 $\times$ 3.2GHz Quad-Core Intel Xeon, 16GB of RAM, mono-core execution. The incompressibility was ensured on about 97000 voxels ($\approx 4\%$ of the image size $171 \times 61 \times 83$). iLog-Demons was about 2 times slower than logDemons but with still reasonable computational time although the algorithm was not at all optimised. i^2LogDemons was too computationally intensive while yielding no significant improvement due to the repeated building, preconditioning and resolution of the linear system (the results are not reported here for the sake of clarity). In iLogDemons, the linear system was built and preconditioned only once, at the beginning of the registration. Similar computation times were obtained for the second patient. Computational performances could be improved using Fourier-based methods (Hinkle et al, 2009) or optimised multi-grid system resolution (Saddi et al, 2007).

6 Discussion and Conclusion

In this article, we presented a method for elastic incompressible diffeomorphic registration based on the logDemons algorithm proposed by Vercauteren et al (2008). We first established that logDemons Gaussian regularisation minimises an infinite order Tikhonov regulariser. Our formulation constitutes a well-posed formulation of demons algorithm with controlled parameters. An important theoretical condition

on the coupling term $\| \log(\phi^{-1} \circ \phi_c)\|^2$ appeared. One must be able to linearise this term such that the regularisation energy is written as a least-square problem to justify the Gaussian regularisation. Equipped with a closed form expression of demons regularisation, we adapted it to elastic registration by replacing the Tikhonov regulariser with the infinite sum of isotropic differential quadratic forms whose minimiser is exactly computed by convolution with the separable elastic-like vector filter proposed by Cachier and Ayache (2004). We then enforced the algorithm to provide incompressible deformations by constraining the search space of the stationary velocities to the space of divergence-free vector fields. In practice, this is achieved by adding a new term to the deformation field estimated by the logDemons. The constraint can therefore be enabled/disabled by the user, so no *ad-hoc* minimisation scheme is required. Compared with traditional methods, our approach is well posed, provides diffeomorphic transformations; introduces only one extra parameter, the elastic parameter κ; and can be applied within a localised area of the image only.

The synthetic experiments demonstrated that the proposed elastic-like regulariser provides realistic elastic deformations with infinite order of smoothness. Contrary to more traditional approaches based on the linear Lamé equation (Modersitzki, 2004), our method relies on separable vector filters that can be implemented using efficient Gaussian filters (Deriche, 1993). As it relies on a kernel, our technique may recall spline-based elastic registration algorithms (Sorzano et al, 2005). However, the transformation provided by the iLogDemons are diffeomorphic and computed everywhere in the image.

In this paper, we used isotropic elastic regularisation to estimate myocardium deformation. Because the cardiac muscle is anisotropic, the regulariser may not be adequate. Yet, designing efficient anisotropic smoothing is not straightforward and, in that case, it is all the more challenging due to the spatial variation of the cardiac anisotropy. We thus decided to use isotropic filters for the sake of efficiency but thanks to the proposed regularisation framework, more advanced anisotropic regularisation could be investigated in the future.

The synthetic experiments also supported the proposed incompressibility constraint. We showed that deformations parameterised by stationary divergence-free velocities are very close to incompressibility despite the approximations and the numerical accuracy. The linearity of the divergence allows efficient implementation of the constraint, in contrast to previous approaches based on the non-linear determinant constraint that were fairly time consuming (Rohlfing et al, 2003; Haber and Modersitzki, 2004). In all our experiments, the Jacobian determinant of the estimated deformations remained close to one independently of the strength of the deformations. We also showed that the i^2LogDemons, which
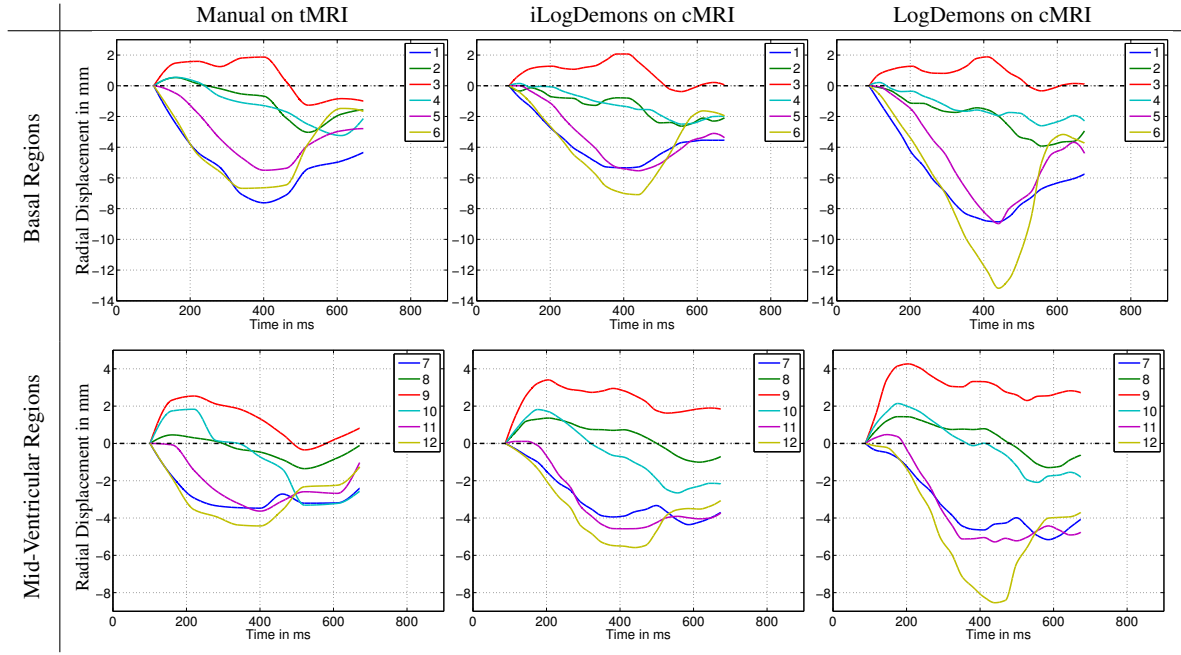
Fig. 13 Regional basal and mid-ventricular radial displacements of patient 2 (in *mm*, colours represent the LV regions). Compared with the radial displacements measured by an expert on tMRI (*left panels*), the displacements estimated on cMRI using iLogDemons (*mid panel*) had more realistic amplitudes compared with those estimated with logDemons (*right panels*). Note that both algorithms recovered realistic radial motion patterns over the cardiac cycle as the image gradients of the cMRI are sufficient to estimate the thickening of the heart.
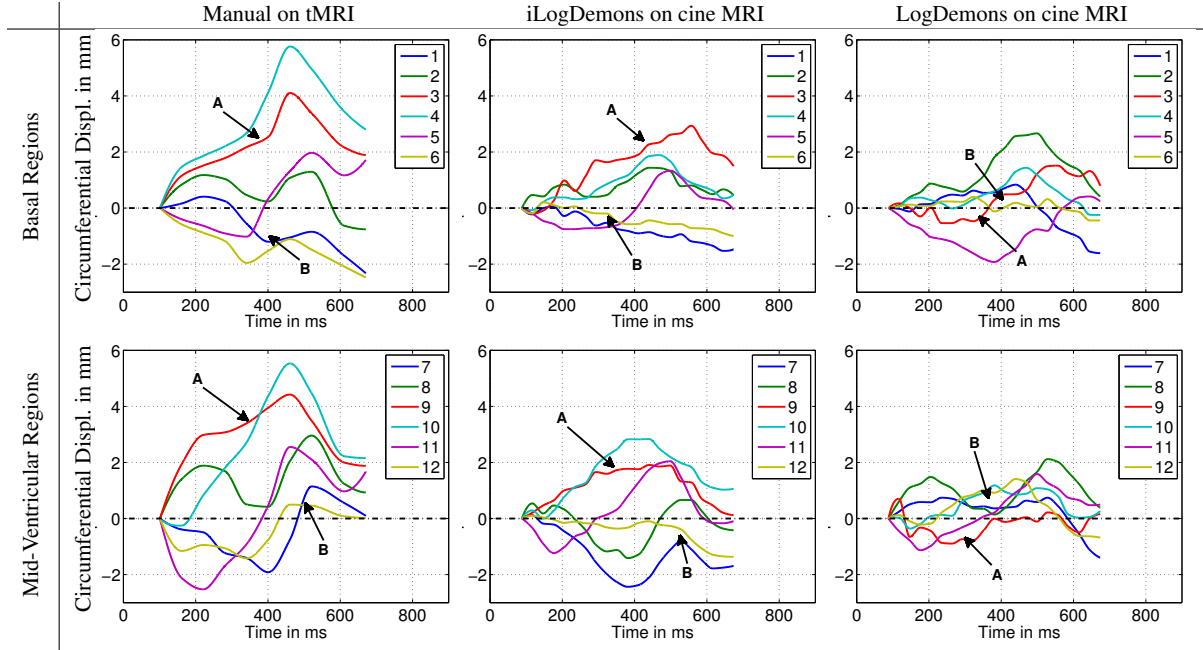

Fig. 14 Regional basal and mid-ventricular circumferential displacements of patient 2 (in *mm*, colours represent the LV regions). Limited by the lack of consistent texture information, the circumferential displacements estimated on cMRI using logDemons (*right panel*) and iLogDemons (*mid panel*) were globally under-estimated compared to tMRI tracking (*left panel*). Yet, iLogDemons displacements presented more realistic patterns, as highlighted by the sign of the displacements of zones 9-10 (A) and zones 7-12 (B) for instance (positive values: counter-clockwise motion).

also constrains the update velocities to be divergence-free, does not significantly improve the recovery of incompressible deformations.

Elastic incompressible registration has numerous clinical applications, from the registration of breast images (Rohlfing et al, 2003) to the tracking of the heart (Bistoquet et al,

2008). In this article, we presented how our approach could be used to estimate 3D myocardium strain from 3D tMRI and standard cMRI of the heart. We observed that enforcing incompressible elasticity significantly increased the realism and the accuracy of the estimated displacements and strains. Recovered deformation fields were closer to those computed automatically or manually from tMRI. The possibility to apply the incompressibility constraint in a limited domain of the image has been crucial for this experiment, as only the myocardium is incompressible. Blood pool volume must vary to ensure correct registration. Moreover, as the myocardium region is relatively small, little computational overhead is added to the logDemons algorithm.

However, some theoretical aspects still need to be consolidated. When the incompressibility constraint is applied within a limited subdomain of the image, smooth transitions are ensured by artificially diffusing the Lagrangian pressure field p. Intuitively, this technique would be equivalent to using a mask of the incompressible domain with smooth transitions. Experiments supported this approach as no numerical instabilities appeared. However, a rigorous formulation that explicitly integrates the mask into the registration energy functional would enable more efficient numerical schemes.

A second theoretical aspect to investigate is the fluid-like, viscous Gaussian regularisation of the update velocities $\delta \mathbf{v}$. Intuitively, this intermediate regularisation controls the regularity of the log-domain, which must be smooth enough to ensure that the integrated transformations are diffeomorphisms (DoCarmo, 1992). Although this step is optional, its use greatly contributes to the stability of the algorithm: A slight smoothing of the update velocities is recommended. It would be interesting however to develop a theoretical proof of this intuition to implement more sophisticated regularisation schemes, by endowing the space of velocity fields with a kernel norm for instance (Hernandez et al, 2009).

Numerically, our approach is relatively simple to implement as it is based on Gaussian filters and it requires solving a linear system with constant stiffness matrix. In this work the Poisson equation was solved in the space domain to be able to constrain incompressibility in regions of arbitrary shapes, which would have been difficult to achieve with Fourier techniques. Nevertheless, elastic-like divergence-free filters implemented in the Fourier domain could be more efficient for whole-domain incompressibility constraint (Hinkle et al, 2009).

In the presented cases and in non reported experiments, no significant effects of the numerical boundary conditions could be observed on the estimated deformations. Yet, numerical instabilities may appear when deformations are strong close to the image boundaries. In these cases, special care should be taken by decreasing the maximum step length λ_x for instance. From a theoretical point of view, a more rigorous implementation of the boundary conditions could be more efficient. Techniques that control the numerical stability automatically (Mansi, 2010) could also be integrated.

As additional future directions, it would be worthwhile to integrate our approach into registration methods based on time-varying velocity fields (Beg et al, 2005; Hinkle et al, 2009). In that respect, it would be interesting to quantitatively evaluate the impact of the stationarity of the velocity on the estimated deformations, although we did not observe any limitations of the algorithm due to that assumption in our experiments. From a clinical point of view, more sophisticated tracking strategies can be investigated to make the estimation of the myocardium motion more robust (Bistoquet et al, 2008; Sundar et al, 2009b). Current work aims to quantitatively validate the algorithm on MRI, 3D US and CT images of healthy subjects and patients suffering from severe congenital heart diseases and heart failure.

A Time-Integration of Stationary Velocity Fields

Arsigny et al (2006a) devised an efficient way to compute the exponential map of a stationary velocity field $\phi = \exp(\mathbf{v})$ by observing that, in virtue of the properties of one-parameter subgroups ($t \mapsto \exp(t\mathbf{v})$), we have $\forall n \in \mathbb{N}, \exp(\mathbf{v}) = \exp(\mathbf{v}/n)^n$. If n is large enough, $\exp(\mathbf{v}/n)$ can be approximated by $\mathbf{v}/n$ (*scaling*), which is then composed $\log_2(n)$ times to get the exponential (*squaring*). The pseudo-code of the algorithm is:

Algorithm 3 Scaling-and-Squaring Algorithm

Require: Velocity field $\mathbf{v}$
1: Choose n such that $\|\mathbf{v}/2^n\| \leq 0.5$
2: Explicit first-order integration: $\mathbf{u} \leftarrow \mathbf{v}/2^n$
3: **loop** {*n times*}
4:    $\mathbf{u} \leftarrow \mathbf{u} \circ \mathbf{u}$
5: **end loop**
6: **return** Displacement field $\mathbf{u}$

B IDQF Parameters for Separable Vector Filters

As described in Sec. 3.2, logDemons elastic-like regularisation is obtained by solving in the Fourier domain the optimal condition:

$$\left[\underbrace{\left(1 + \sum_{k=1}^{\infty} \frac{\alpha_k (\mathbf{w}^T \mathbf{w})^k}{\lambda_d^{2k}} \right)}_{A} \mathrm{Id} + \underbrace{\left(\sum_{k=1}^{\infty} \frac{\beta_k (\mathbf{w}^T \mathbf{w})^{k-1}}{\lambda_d^{2k}} \right)}_{B} \mathbf{w}\mathbf{w}^T \right] \hat{\mathbf{v}}(\mathbf{w}) = \hat{\mathbf{v}}_c(\mathbf{w})$$

Sherman-Morrison inversion Lemma gives:

$$\hat{\mathbf{v}}(\mathbf{w}) = \underbrace{\left[\frac{1}{A}\mathrm{Id} - \frac{1}{A}\left(\frac{B}{A+B\mathbf{w}^T\mathbf{w}}\right)\mathbf{w}\mathbf{w}^T\right]}_{M}\hat{\mathbf{v}}_c(\mathbf{w})$$

We seek α_k and β_k such that the filter M is separable to preserve demons computational efficiency. $\alpha_k = 1/k!$ yields $A = \exp(\mathbf{w}^T\mathbf{w}/\lambda_d^2)$. As a result, if $B/(A+B\mathbf{w}^T\mathbf{w})$ is a scalar $\gamma \in \mathbb{R}$, the inverse Fourier transform of the second term of M is the Hessian of $\mathfrak{F}^{-1}(\gamma\exp(-\mathbf{w}^T\mathbf{w}/\lambda_d^2))$. The idea thus consists in finding the coefficients β_k such that $B/(A+B\mathbf{w}^T\mathbf{w}) = \gamma$. With $\beta_0 = 0$, this writes:

$$\sum_{k=0}^{\infty}\frac{\beta_{k+1}}{\lambda_d^{2(k+1)}}(\mathbf{w}^T\mathbf{w})^k = \sum_{k=0}^{\infty}\gamma\left(\frac{1}{\lambda_d^{2k}k!} + \frac{\beta_k}{\lambda_d^{2k}}\right)(\mathbf{w}^T\mathbf{w})^k$$

This equation defines a recursive relationship between the β_k's:

$$\begin{cases}\beta_0 = 0 \\ \beta_{k+1} = \gamma\left(\dfrac{\lambda_d^2}{k!} + \beta_k\right) \qquad \forall k \geq 1\end{cases}$$

from which we deduce the closed form:

$$\beta_k = \sum_{i=1}^{k}\frac{\gamma^i\lambda_d^{2i}}{(k-i)!}$$

The proof of this relationship is achieved by recurrence. The previous formula is verified for $k = 1$. We assume it to be true for k and we verify it still holds for $k+1$. To this end, we replace β_k by the conjectured formula in the recursive expression of β_{k+1}:

$$\beta_{k+1} = \lambda_d^2\gamma\left(\frac{1}{k!} + \sum_{i=1}^{k}\frac{\gamma^i\lambda_d^{2i}}{(k-i)!}\right) = \frac{\gamma\lambda_d^2}{k!} + \sum_{i=1}^{k}\frac{\gamma^{i+1}\lambda_d^{2(i+1)}}{(k-i)!}$$

$$= \frac{\gamma\lambda_d^2}{k!} + \sum_{i=2}^{k+1}\frac{\gamma^i\lambda_d^{2i}}{(k-(i-1))!} = \sum_{i=1}^{k+1}\frac{\gamma^i\lambda_d^{2i}}{(k+1-i)!}$$

which proves the result. With these coefficients, the filter M writes:

$$\hat{\mathbf{v}}(\mathbf{w}) = \left(\exp(-\mathbf{w}^T\mathbf{w}/\lambda_d^2)\,\mathrm{Id} - \gamma\mathbf{w}\mathbf{w}^T\exp(-\mathbf{w}^T\mathbf{w}/\lambda_d^2)\right)\star\hat{\mathbf{v}}_c(\mathbf{w})$$

which becomes in the space domain (Δ is the Hessian operator and d is the dimension of the image domain Ω)

$$\mathbf{v}(\mathbf{x}) = \sqrt{\lambda_d^2/(4\pi)}^d\exp(-4\lambda_d^2\mathbf{x}^T\mathbf{x})\star\mathbf{v}_c(\mathbf{x})$$

$$+ \gamma\Delta\left(\sqrt{\lambda_d^2/(4\pi)}^d\exp(-4\lambda_d^2\mathbf{x}^T\mathbf{x})\right)\star\mathbf{v}_c(\mathbf{x})$$

Defining $\sigma_{el}^2 = 2/\lambda_d^2$ and $\gamma = \sigma_{el}^2\kappa/(1+\kappa)$ yields (9).

C Demons Update Velocity under the Divergence-Free Constraint

Divergence-free update velocities are computed by minimising the constrained optimisation energy:

$$\begin{cases}\mathscr{E}_{cor}(\delta\mathbf{v}) = \dfrac{1}{\lambda_i^2}\|R - T\circ\phi\circ\exp(\delta\mathbf{v})\|_{L_2}^2 + \dfrac{1}{\lambda_x^2}\|\log(\phi^{-1}\circ\phi\circ\exp(\delta\mathbf{v}))\|_{L_2}^2 \\ \nabla\cdot\delta\mathbf{v} = 0\end{cases}$$

Let $p(\mathbf{x})$ be a scalar field with compact support. The Lagrangian function $\mathscr{P}_{corr}(\delta\mathbf{v}, p)$ related to the constrained correspondence energy

$\mathscr{E}_{corr}(\delta\mathbf{v})$ writes (the Lagrangian multiplier $p(\mathbf{x})$ has been multiplied by 2 to simplify calculations):

$$\mathscr{P}_{corr}(\delta\mathbf{v}, p) = \frac{1}{\lambda_i^2}\int_\Omega\|R(\mathbf{x}) - T\circ\phi\circ\exp\delta\mathbf{v}(\mathbf{x})\|^2\,\mathrm{d}\mathbf{x}$$

$$+ \frac{1}{\lambda_x^2}\int_\Omega\|\delta\mathbf{v}(\mathbf{x})\|^2\,\mathrm{d}\mathbf{x} - 2\int_\Omega p(\mathbf{x})\,\nabla\cdot\delta\mathbf{v}(\mathbf{x})\mathrm{d}\mathbf{x}$$

Differentiating $\mathscr{P}_{corr}(\delta\mathbf{v}, p)$ with respect to p yields the constraint $\nabla\cdot\delta\mathbf{v} = 0$. To differentiate $\mathscr{P}_{corr}(\delta\mathbf{v}, p)$ with respect to $\delta\mathbf{v}$, we linearise the similarity criterion as in (Vercauteren et al, 2009):

$$\|R(\mathbf{x}) - T\circ\phi\circ\exp\delta\mathbf{v}(\mathbf{x})\|^2 \approx \|R(\mathbf{x}) - T\circ\phi(\mathbf{x}) + J(\mathbf{x})^T\,\delta\mathbf{v}(\mathbf{x})\|^2$$

where $J(\mathbf{x})$ is the symmetric gradient $J(\mathbf{x}) = (\nabla R(\mathbf{x}) + \nabla(T\circ\phi)(\mathbf{x}))/2$. It follows the linear least square problem:

$$\mathscr{P}_{corr}(\delta\mathbf{v}, p) = \frac{1}{\lambda_i^2}\int_\Omega\|R(\mathbf{x}) - T\circ\phi(\mathbf{x}) + J(\mathbf{x})^T\delta\mathbf{v}(\mathbf{x})\|^2\mathrm{d}\mathbf{x}$$

$$+ \frac{1}{\lambda_x^2}\int_\Omega\|\delta\mathbf{v}(\mathbf{x})\|^2\mathrm{d}\mathbf{x} - 2\int_\Omega p(\mathbf{x})\,\nabla\cdot\delta\mathbf{v}(\mathbf{x})\mathrm{d}\mathbf{x}$$

The optimal condition $\partial_{\delta\mathbf{v}}\mathscr{P}_{corr}(\delta\mathbf{v}, p) = 0$ thus writes:

$$\underbrace{\left(J(\mathbf{x})J(\mathbf{x})^T + \frac{\lambda_i^2}{\lambda_x^2}\,\mathrm{Id}\right)}_{D(\mathbf{x})}\delta\mathbf{v}(\mathbf{x}) = -J(\mathbf{x})\left(R(\mathbf{x}) - T\circ\phi(\mathbf{x})\right) - \lambda_i^2\nabla p(\mathbf{x})$$

As the tensor $D(\mathbf{x})$ is always invertible, we can calculate the optimal divergence-free update velocity field:

$$\delta\mathbf{v}^*(\mathbf{x}) = \underbrace{-\left(R(\mathbf{x}) - T\circ\phi(\mathbf{x})\right)D(\mathbf{x})^{-1}J(\mathbf{x})}_{\delta\mathbf{v}(\mathbf{x})} - \lambda_i^2 D(\mathbf{x})^{-1}\nabla p(\mathbf{x}) \quad (14)$$

The first term of the previous equation is exactly the logDemons update velocity field $\delta\mathbf{v}$ (3).The pressure field p is calculated by solving the Poisson equation under 0-Dirichlet boundary conditions that results from the divergence of the previous equation:

$$\nabla\cdot\left(\lambda_i^2 D(\mathbf{x})^{-1}\nabla p(\mathbf{x})\right) = \nabla\cdot\delta\mathbf{v}(\mathbf{x})$$

Because the tensor $D(\mathbf{x})$ is updated at each iteration, the operator $\nabla\cdot(\lambda_i^2 D^{-1}\nabla)$ is not constant. The matrix of the related linear system must therefore be built and pre-conditioned at each time step, which can be computationally demanding if the domain Ω is large. Furthermore, $D(\mathbf{x})$ is computed at every voxel of the image domain Ω independently. The resulting tensor field can therefore be noisy, likely yielding numerical instabilities. To alleviate this limitation, D is smoothed using Log-Euclidian techniques (Arsigny et al, 2006b): each component of $\log(D)$ is smoothed with a Gaussian kernel G_{λ_d} and the result is exponentiated to get a smooth tensor field. In this paper, we fixed λ_d^2 equal to the strength σ_{fl}^2 of the fluid regularisation.

D Robustness of iLogDemons with Respect to the Slice Thickness

During our experiments we also quantified the robustness of the iLogDemons with respect to image slice thickness on synthetic data. The reference and the warped images of the whirl data sets were degraded by artificially increasing the slice thickness along the z-axis. Every N consecutive slices were grouped together and averaged to simulate partial volume effect. In-plane resolution was preserved. The resulting images were resampled to get $1\,mm^3$-isotropic voxels. Four datasets were generated with slice thicknesses spanning from $1\,mm$ to $10\,mm$. The

registration parameters were $\sigma_{fl}^2 = 1$, $\sigma_{el}^2 = 1$ and $\lambda_x = 1$. Results are reported in Fig. 15.

Not surprisingly, increasing the slice thickness decreased the overall registration accuracy as less image information was available: RMSE and DTF steadily increased. LogDemons yielded better image matching (lower RMSE) but the recovered deformation fields were less accurate than those estimated using iLogDemons (higher DTF). Incompressibility constraints helped the algorithm to recover the incompressible whirl. This experiment also confirmed that i^{2}Logdemons did not improve registration accuracy with respect to iLogDemons. Fig. 16 illustrates these findings on a particular case. Far from image gradients, the deformation estimated by logDemons were weak and erroneous (arrow A). Even worse, near strong image gradients, the deformation field can be completely wrong (arrow B). Thanks to the incompressibility constraint, iLogDemons alleviated these pitfalls and recovered a plausible through-plane motion (arrow C). These results motivate the use of iLogDemons to estimate the motion of incompressible organs in medical images.
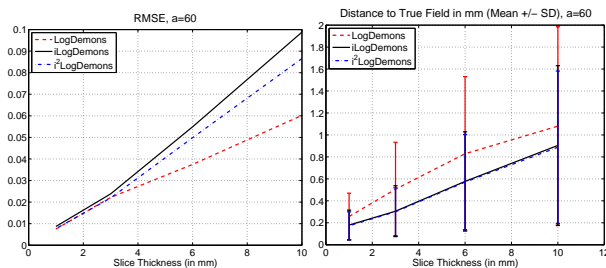

Fig. 15 RMSE and DTF with respect to the slice thickness. Despite higher RMSE, estimated deformation fields were systematically more accurate using incompressible constraints (iLogDemons) than using logDemons. One can also see that constraining the update velocity to be divergence-free (i^{2}LogDemons) did not improve the results in terms of DTF. Same conclusions for all the other whirl angles.
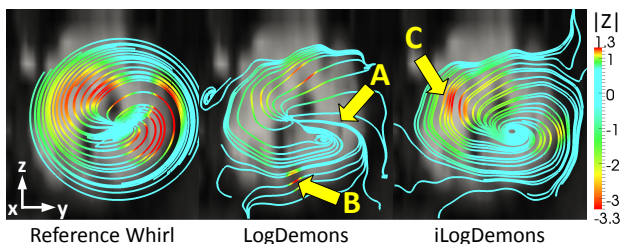

Fig. 16 Streamlines of 3D whirl transformations ($\alpha_0 = 60°$) recovered from an image with 6mm-thick slices. Contrary to logDemons, which failed to recover the whirl transformation in homogeneous regions (A) and was misguided by strong gradients (B), iLogDemons improved the recovery of the through-plane whirl deformations (C) despite the lack of image information. Colours encode the amplitude of the through-plane z-direction in mm.

References

Arnold V (1989) Mathematical methods of classical mechanics. Springer-Verlag

Arsigny V, Commowick O, Pennec X, Ayache N (2006a) A log-euclidean framework for statistics on diffeomorphisms. In: Medical Image Computing and Computer Assisted Intervention (MICCAI), Springer, Lecture Notes in Computer Science, vol 4190, p 924

Arsigny V, Fillard P, Pennec X, Ayache N (2006b) Log-Euclidean metrics for fast and simple calculus on diffusion tensors. Magnetic Resonance in Medicine 56(2):411–421

Ashburner J (2007) A fast diffeomorphic image registration algorithm. Neuroimage 38(1):95–113

Ashburner J, Hutton C, Frackowiak R, Johnsrude I, Price C, Friston K (1998) Identifying global anatomical differences: deformation-based morphometry. Human Brain Mapping 6(5-6):348–357

Beg M, Miller M, Trouvé A, Younes L (2005) Computing Large Deformation Metric Mappings via Geodesic Flows of Diffeomorphisms. International Journal of Computer Vision 61(2):139–157

Bistoquet A, Oshinski J, Skrinjar O (2008) Myocardial deformation recovery from cine MRI using a nearly incompressible biventricular model. Medical Image Analysis 12(1):69–85

Bossa M, Hernandez M, Olmos S (2007) Contributions to 3D diffeomorphic atlas estimation: application to brain images. In: Medical Image Computing and Computer Assisted Intervention (MICCAI), Springer, Lecture Notes in Computer Science, vol 10, p 667

Broit C (1981) Optimal registration of deformed images. PhD thesis, University of Pennsylvania Philadelphia, PA, USA

Cachier P, Ayache N (2004) Isotropic energies, filters and splines for vectorial regularization. J of Math Imaging and Vision 20(3):251–265

Cachier P, Pennec X, Ayache N (1999) Fast Non Rigid Matching by Gradient Descent: Study and Improvements of the Demons Algorithm. Tech. Report RR-3706, INRIA

Cachier P, Bardinet E, Dormont D, Pennec X, Ayache N (2003) Iconic feature based nonrigid registration: the PASHA algorithm. Computer Vision and Image Understanding 89(2-3):272–298

Cahill ND, Noble JA, Hawkes DJ (2009) A demons algorithm for image registration with locally adaptive regularization. In: Medical Image Computing and Computer Assisted Intervention (MICCAI), Springer, Lecture Notes in Computer Science, vol 5761, pp 574–581

Choi Y, Lee S (2000) Injectivity conditions of 2D and 3D uniform cubic b-spline functions. Graphical Models 62:2000

Clatz O, Delingette H, Talos I, Golby A, Kikinis R, Jolesz F, Ayache N, Warfield S (2005) Robust nonrigid registration to capture brain shift from intraoperative MRI. IEEE Transactions on Medical Imaging 24(11):1417–1427

Cuzol A, Hellier P, Mémin E (2007) A low dimensional fluid motion estimator. International Journal of Computer Vision 75(3):329–349

DeCraene M, Camara O, Bijnens B, Frangi A (2009) Large diffeomorphic ffd registration for motion and strain quantification from 3d-us sequences. In: Functional Imaging and Modeling of the Heart (FIMH), Springer-Verlag, Lecture Notes in Computer Science, vol 5528, pp 437–446

Deriche R (1993) Recursively implementing the gaussian and its derivatives. Rapports de recherche- INRIA

DoCarmo M (1992) Riemannian Geometry (transl. by Francis Flaherty), Math. Theory Appl. Birkhäuser Boston, Inc., Boston, MA

Dru F, Vercauteren T (2009) An ITK implementation of the symmetric log-domain diffeomorphic demons algorithm. Insight Journal – 2009 January - June

Evans LC (1998) Partial Differential Equations. American Mathematical Society

Ferrant M, Nabavi A, Macq B, Jolesz F, Kikinis R, Warfield S (2001) Registration of 3D intraoperative MR images of the brain using a finite element biomechanical model. IEEE Transactions on Medical Imaging 20(12):1384–1397

Glass L, Hunter P, McCulloch A (1991) Theory of Heart: Biomechanics, Biophysics, and Nonlinear Dynamics of Cardiac Function. Springer-Verlag

Glockner H (2006) Fundamental problems in the theory of infinite-dimensional lie groups. Arxiv preprint math/0602078

Gorce J, Friboulet D, Magnin I (1997) Estimation of three-dimensional cardiac velocity fields: assessment of a differential method and application to three-dimensional CT data. Medical Image Analysis 1(3):245–261

Haber E, Modersitzki J (2004) Numerical methods for volume preserving image registration. Inverse Problems 20(5):1621–1638

Heitz D, Mémin E, Schnörr C (2009) Variational fluid flow measurements from image sequences: synopsis and perspectives. Experiments in Fluids pp 1–25

Hernandez M, Bossa M, Olmos S (2009) Registration of anatomical images using paths of diffeomorphisms parameterized with stationary vector field flows. International Journal of Computer Vision 85(3):291–306

Hinkle J, Fletcher P, Wang B, Salter B, Joshi S (2009) 4D MAP Image Reconstruction Incorporating Organ Motion. In: Proceedings of the 21st International Conference on Information Processing in Medical Imaging, Springer, p 687

Horn B, Schunck B (1981) Determining optical flow. Artificial intelligence 17(1-3):185–203

Lorenzi M, Ayache N, Frisoni G, Pennec X (2010) 4D registration of serial brain MR's images: a robust measure of changes applied to Alzheimer's disease. In: MICCAI STIA Workshop, Beijing, China

Mansi T (2010) Image-Based Physiological and Statistical Models of the Heart, Application to Tetralogy of Fallot. Thèse de sciences (PhD thesis), Ecole Nationale Supérieure des Mines de Paris

Mansi T, Peyrat JM, Sermesant M, Delingette H, Blanc J, Boudjemline Y, Ayache N (2009) Physically-Constrained Diffeomorphic Demons for the Estimation of 3D Myocardium Strain from Cine-MRI. In: Proceedings of Functional Imaging and Modeling of the Heart 2009 (FIMH'09), Lecture Notes in Computer Science, vol 5528, pp 201–210

Miller MI, Trouvé A, Younes L (2002) On the metrics and Euler-Lagrange equations of computational anatomy. Annual Review of Biomed Eng 4:375–405

Modersitzki J (2004) Numerical Methods for Image Registration. Oxford University Press

Moore C, Lugo-Olivieri C, McVeigh E, Zerhouni E (2000) Three-dimensional systolic strain patterns in the normal human left ventricle: Characterization with tagged MR imaging. Radiology 214(2):453–466

Nielsen M, Florack L, Deriche R (1994) Regularization and scale space. Tech. report, INRIA

Papademetris X, Sinusas A, Dione D, Constable R, Duncan J (2000) Estimating 3D strain from 4D cine-MRI and echocardiography: In-vivo validation. In: Medical Image Computing and Computer Assisted Intervention (MICCAI), Springer, Lecture Notes in Computer Science, pp 678–686

Pennec X, Cachier P, Ayache N (1999) Understanding the demon's algorithm: 3D non-rigid registration by gradient descent. In: Medical Image Computing and Computer Assisted Intervention (MICCAI), Springer, Cambridge, UK, Lecture Notes in Computer Science, vol 1679, pp 597–605

Peyrat JM, Delingette H, Sermesant M, Xu C, Ayache N (2009) Registration of 4d cardiac ct sequences under trajectory constraints with multichannel diffeomorphic demons. IEEE Transactions on Medical Imaging

Phatak N, Maas S, Veress A, Pack N, Di Bella E, Weiss J (2009) Strain measurement in the left ventricle during systole with deformable image registration. Medical Image Analysis 13:354–361

Rohlfing T, Maurer Jr C, Bluemke D, Jacobs M (2003) Volume-preserving nonrigid registration of MR breast images using free-form deformation with an incompressibility constraint. IEEE Transactions on Medical Imaging 22(6):730–741

Rueckert D, Sonoda L, Hayes C, Hill D, Leach M, Hawkes D (1999) Nonrigid registration using free-form deformations: application to breast MR images. IEEE Transactions on Medical Imaging 18(8):712–721

Rueckert D, Aljabar P, Heckemann R, Hajnal J, Hammers A (2006) Diffeomorphic registration using b-splines. In: Medical Image Computing and Computer Assisted Intervention (MICCAI), Springer, Lecture Notes in Computer Science, vol 9, p 702

Saddi KA, Chefd'hotel C, Cheriet F (2007) Large deformation registration of contrast-enhanced images with volume-preserving constraint. In: Proceedings of SPIE Medical Imaging, SPIE, vol 6512

Simard PY, Mailloux GE (1988) A projection operator for the restoration of divergence-free vector fields. IEEE Transactions on Pattern Analysis and Machine Intelligence 10(2):248–256

Sinusas A, Papademetris X, Constable R, Dione D, Slade M, Shi P, Duncan J (2001) Quantification of 3-D regional myocardial deformation: shape-based analysis of magnetic resonance images. American Journal of Physiology- Heart and Circulatory Physiology 281(2):698–714

Song S, Leahy R (1991) Computation of 3-D velocity fields from 3-D cine CT images of a human heart. IEEE Transactions on Medical Imaging 10(3):295–306

Sorzano C, Thévenaz P, Unser M (2005) Elastic registration of biological images using vector-spline regularization. IEEE Transactions on Biomedical Engineering 52(4):652–663

Sundar H, Davatzikos C, Biros G (2009a) Biomechanically-Constrained 4D Estimation of Myocardial Motion. In: Medical Image Computing and Computer Assisted Intervention (MICCAI), Springer, Lecture Notes in Computer Science, vol 5762, pp 257–265

Sundar H, Littb H, Shena D (2009b) Estimating myocardial motion by 4d image warping. Pattern Recognition 42:2514–2526

Thirion JP (1998) Image matching as a diffusion process: an analogy with Maxwell's demons. Medical Image Analysis pp 243–260

Vercauteren T, Pennec X, Perchant A, Ayache N (2008) Symmetric log-domain diffeomorphic registration: A demons-based approach. In: Medical Image Computing and Computer Assisted Intervention (MICCAI), Springer-Verlag, New York, USA, Lecture Notes in Computer Science, vol 5241, pp 754–761

Vercauteren T, Pennec X, Perchant A, Ayache N (2009) Diffeomorphic demons: Efficient non-parametric image registration. NeuroImage 45(1S1):61–72

Veress A, Gullberg G, Weiss J (2005) Measurement of Strain in the Left Ventricle during Diastole with cine-MRI and Deformable Image Registration. Journal of Biomechanical Engineering 127:1195

Yeo B, Vercauteren T, Fillard P, Peyrat J, Pennec X, Golland P, Ayache N, Clatz O (2009) DT-REFinD: Diffusion tensor registration with exact finite-strain differential. IEEE Transactions on Medical Imaging 28(12):1914–1928